IAEA nuclear fusion

PAPER • OPEN ACCESS

Experiments in high-performance JET plasmas in preparation of second harmonic ICRF heating of tritium in ITER

To cite this article: M.J. Mantsinen *et al* 2023 *Nucl. Fusion* **63** 112015

OPEN ACCESS
IOP Publishing | International Atomic Energy Agency
Nuclear Fusion
Nucl. Fusion **63** (2023) 112015 (20pp)
https://doi.org/10.1088/1741-4326/aceb08

Experiments in high-performance JET plasmas in preparation of second harmonic ICRF heating of tritium in ITER

M.J. Mantsinen[1,2,*], P. Jacquet[3], E. Lerche[3,4], D. Gallart[1], K. Kirov[3], P. Mantica[5], D. Taylor[3], D. Van Eester[4], M. Baruzzo[6], I. Carvalho[3], C.D. Challis[3], A. Dal Molin[5], E. Delabie[7], E. De La Luna[8], R. Dumont[9], P. Dumortier[4], J. Eriksson[10], D. Frigione[11], J. Garcia[9], L. Garzotti[3], C. Giroud[3], R. Henriques[3], J. Hobirk[12], A. Kappatou[12], Y. Kazakov[4], D. Keeling[3], D. King[3], V. Kiptily[3], M. Lennholm[3], P. Lomas[3], C. Lowry[13], C.F. Maggi[3], J. Mailloux[3], M. Maslov[3], S. Menmuir[3], I. Monakhov[3], R.B. Morales[3], C. Noble[3], M. Nocente[5,14], A. Patel[3], G. Pucella[6], C. Reux[9], D. Rigamonti[5], F. Rimini[3], A. Sheikh[3], S. Silburn[3], P. Siren[3], E.R. Solano[8], Z. Stancar[3,15], M. Tardocchi[5] and JET Contributors[a]

[1] Barcelona Supercomputing Center, Barcelona, Spain
[2] ICREA, Barcelona, Spain
[3] United Kingdom Atomic Energy Authority, Culham Science Centre, Abingdon, Oxon OX14 3DB, United Kingdom of Great Britain and Northern Ireland
[4] Laboratory for Plasma Physics, ERM/KMS, B-1000 Brussels, Belgium
[5] Institute of Plasma Science and Technology, CNR, 20125 Milano, Italy
[6] ENEA, Fusion and Nuclear Safety Department, C.R. Frascati, 00044 Frascati, Italy
[7] Oak Ridge National Laboratory, Oak Ridge, TN 37830, United States of America
[8] Laboratorio Nacional de Fusión, CIEMAT, 28040 Madrid, Spain
[9] CEA, IRFM, F-13108 St-Paul-Lez-Durance, France
[10] Department of Physics and Astronomy, Uppsala University, 75120 Uppsala, Sweden
[11] University of Tor Vergata, Rome, Italy
[12] Max-Planck-Institut für Plasmaphysik, Boltzmannstr. 2, 85748 Garching, Germany
[13] European Commission, B-1049 Brussels, Belgium
[14] Dipartimento di Fisica 'G. Occhialini', Università di Milano-Bicocca, Milano, Italy
[15] Slovenian Fusion Association (SFA), Jozef Stefan Institute, SI-1000 Ljubljana, Slovenia

E-mail: mervi.mantsinen@bsc.es

Received 13 March 2023, revised 3 July 2023
Accepted for publication 27 July 2023
Published 12 October 2023

Abstract

The reference ion cyclotron resonance frequency (ICRF) heating schemes for ITER deuterium–tritium (D-T) plasmas at the full magnetic field of 5.3 T are second harmonic heating of T and ^{3}He minority heating. The wave-particle resonance location for these schemes coincide and are central at a wave frequency of 53 MHz at 5.3 T. Experiments have been carried out in

[a] See the author list of "Overview of T and D-T results in JET with ITER-like wall" by C.F. Maggi *et al* to be published in *Nuclear Fusion Special Issue: Overview and Summary Papers from the 29th Fusion Energy Conference (London, UK, 16–21 October 2023)*.
[*] Author to whom any correspondence should be addressed.

the second major D-T campaign (DTE2) at JET, and in its prior D campaigns, to integrate these ICRF scenarios in JET high-performance plasmas and to compare their performance with the commonly used hydrogen (H) minority heating. In 50:50 D:T plasmas, up to 35% and 5% larger fusion power and diamagnetic energy content, respectively, were obtained with second harmonic heating of T as compared to H minority heating at comparable total input powers and gas injection rates. The core ion temperature was up to 30% and 20% higher with second harmonic T and ^{3}He minority heating, respectively, with respect to H minority heating. These are favourable results for the use of these scenarios in ITER and future fusion reactors. According to modelling, adding ICRF heating to neutral beam injection using D and T beams resulted in a 10%–20% increase of on-axis bulk ion heating in the D-T plasmas due to its localisation in the plasma core. Central power deposition was confirmed with the break-in-slope and fast Fourier transform analysis of ion and electron temperature in response to ICRF modulation. The tail temperature of fast ICRF-accelerated tritons, their enhancement of the fusion yield and time behaviour as measured by an upgraded magnetic proton recoil spectrometer and neutral particle analyser were found in agreement with theoretical predictions. No losses of ICRF-accelerated ions were observed by fast ion detectors, which was as expected given the high plasma density of $n_e \approx 7–8 \times 10^{19}$ m^{-3} in the main heating phase that limited the formation of ICRF-accelerated fast ion tails. ^{3}He was introduced in the machine by ^{3}He gas injection, and the ^{3}He concentration was measured by a high-resolution optical penning gauge in the sub-divertor region. The DTE2 experiments with ^{3}He minority heating were carried with a low ^{3}He concentration in the range of 2%–4% given the fact that the highest neutron rates with ^{3}He minority heating in D plasmas were obtained at low ^{3}He concentrations of $\sim$2%, which also coincided with the highest plasma diamagnetic energy content. In addition to ^{3}He introduced by ^{3}He gas injection, an intrinsic concentration of ^{3}He of the order of 0.2%–0.4% was measured in D-T plasmas before ^{3}He was introduced in the device, which is attributed to the radioactive decay of tritium to ^{3}He. According to modelling, even such low intrinsic concentrations of ^{3}He lead to significant changes in ICRF power partitioning during second harmonic heating of T due to absorption of up to 30% of the wave power by ^{3}He.

Keywords: ICRF heating, fast ions, computational modelling, JET tokamak, H-mode hybrid plasma scenario, deuterium–tritium fuel mixture

1. Introduction

The reference ion cyclotron resonance frequency (ICRF) heating schemes for ITER deuterium–tritium (D-T) plasmas at the full magnetic field of 5.3 T are second harmonic heating of tritium and ^{3}He minority heating. The wave-particle resonance location for these schemes coincide and are central at a wave frequency of 53 MHz at 5.3 T [1]. Experimental studies of these heating schemes have been limited so far due to the scarcity of D-T plasmas. In 1994, they were investigated in TFTR D-T supershot plasmas and resulted in an increase in the ion temperature, electron temperature and fusion yield [2, 3]. In the first major D-T campaign (DTE1) at JET in 1997, these heating schemes were mainly tested in ICRF-only H-mode plasmas [4–6] where ^{3}He minority heating was found to result in a higher ion temperature, plasma energy content and fusion yield as compared to second harmonic heating of tritium without ^{3}He gas injection. Fast triton losses were considered as the main factor limiting the performance of second harmonic heating of tritium given the relatively low plasma densities. However, no fast ion loss detectors (FILDs) were available at the time to confirm this hypothesis. Apart from the experiments in ICRF-only H-mode plasmas, few attempts were made using these schemes with dual-frequency ICRF operation together with hydrogen minority heating in ELM-free H-modes [7] in the JET DTE1 campaign. Thereafter, it took until the second major D-T campaign (DTE2) of JET in 2021 before it was possible to carry out further experiments with these ICRF scenarios in D-T plasmas. This paper reports on the experiments carried out in DTE2 to integrate these ICRF scenarios in high-performance plasmas and to compare their performance with respect to that of the commonly used hydrogen minority heating. Since these experiments were carried out in high-performance H-mode plasma conditions and a beryllium/tungsten environment, they provide information on the performance of these ICRF schemes in conditions that are closer to ITER than was possible to obtain in the earlier JET DTE1 ICRF-only experiments [4–6]. The main challenge of these experiments was related to the reproducibility of experimental conditions to allow comparisons of the different ICRF heating schemes.

The JET DTE1 campaign in 1997 was carried out with the Mark IIAP single-null divertor configuration, which comprised carbon/carbon-fibre-composite tiles mounted on a water cooled support structure [8]. The remainder of the first wall was protected with carbon tiles, and all surfaces were periodically coated with thin Be films. With respect to DTE1, several upgrades to JET were made prior to DTE2 including the ITER-like wall (ILW consisting of a beryllium first wall and a tungsten divertor) installed in 2010, improved diagnostic capabilities and a neutral beam injection (NBI) upgrade in 2019–2020 [9]. Given these enhancements and fast-ions diagnostic improvements [10–12], DTE2 provided a good opportunity to further characterise ICRF scenarios in preparation of the ITER program. A number of high-priority issues related to ITER ICRF D-T scenarios were identified and investigated in DTE2. They included:

- Optimising the use of ITER ICRF scenarios in high-performance D-T plasmas for high fusion performance.
- Improving heating performance of $\omega = 2\,\omega(\mathrm{T})$ relative to DTE1 results in D-T plasmas.
- Studying transition from dominant $\omega = \omega(^3\mathrm{He})$ absorption to $\omega = 2\,\omega(\mathrm{T})$ damping in D-T plasmas.

The DTE2 experiments reported in this paper addressed these high-priority issues using a hybrid target plasma [13–15]. The experiments carried out using ^{3}He minority heating in high-performance D plasmas in preparation of the DTE2 experiments are also reported while experiments on D minority ICRF heating in DTE2 which yielded the new fusion energy record and those using three ion ICRF schemes in DTE2 are reported in [16, 17] and [18], respectively. The experiments in D plasmas with ^{3}He minority heating are included because they not only guided the preparation of the DTE2 experiments but also supported our conclusions from them. Prior to DTE2, extensive modelling was undertaken to prepare and support the experimental work, see e.g. [19–25]. ICRF modelling has been carried out mainly with PION [26], TORIC [27] within TRANSP [28] and CYRANO [29]. The PION code provides self-consistent time-dependent modelling of ICRF power deposition and distribution functions of resonating ions using simplified models, including NBI + ICRF synergy [30]. TORIC within TRANSP and CYRANO modelling include a full-wave solver and a Fokker Planck module. PION and TRANSP were used for modelling of many DTE1 experiments involving ICRF heating [4–7, 31] and overall, good agreement with experiments was found.

The rest of this paper is organised as follows: in section 2, the physics basis for ICRF heating schemes used in JET high-performance DTE2 discharges are briefly presented. In section 3, the overview of the experimental set-up is given. In sections 4 and 5, the results are presented for D-T and D plasmas, respectively. Finally, section 6 provides the discussion and conclusions.

2. Physics basis for ICRF heating schemes used in JET high-performance DTE2 discharges

During ICRF heating the wave energy is absorbed by ions when the Doppler-shifted wave angular frequency ω matches the ion cyclotron angular frequency ω_{ci} or its harmonic. In many cases the Doppler shift is relatively small, the resonance condition reduces to $\omega = n\omega_{\mathrm{ci}},\ n \geqslant 1$. Consequently, the power deposition becomes strongly localised in the region where $\omega \approx n\omega_{\mathrm{ci}}$. Since ω_{ci} scales as 1/B, the location of the absorption can be externally controlled by matching the wave frequency according to the known magnetic field B. For the fast wave, the wave electric field parallel to the background magnetic field is relatively small, and we can divide the electric field component perpendicular to the background magnetic field into two components: one component, E_+, rotates in the same direction as the ions and the other component, E_-, is counter-rotating. To first order, it is the E_+ component of the fast wave that gives rise to absorption by resonating ions. There are several well-known ways to obtain a favourable polarisation for efficient wave damping by resonant ions. One option is to use the harmonics of the ion cyclotron frequency, for which $|E_+/E_-| = (n-1)/(n+1)$. Another possibility is to work in the minority heating regime [32]. In the minority heating regime, the dispersion of the wave is in first approximation determined by the majority ion species, and the minority ion species can be heated, provided the fundamental ion cyclotron resonance of the minority ions resides in the plasma. In so called three-ion schemes [33], the minority heating resonance is located in the region of the enhanced E_+ at the mode conversion layer between two main ion species.

Hydrogen as a minority in a tokamak plasma minimises fuel dilution. This, together with the favourable E_+ polarisation, make hydrogen ions a natural choice for a minority species to be heated by ICRF waves for high-performance JET D, T or D-T discharges. In the case of H minority heating, the single-pass absorption is usually high, but the drawback, especially in the case of a low minority hydrogen concentration and low plasma density, is that the bulk ion heating tends to be modest, as the minority hydrogen ions often are accelerated to high energies and slow down on electrons. A ^{3}He minority (i.e. ^{3}He injected in the plasma) is preferred in some experiments because of its better bulk ion heating properties thanks to a higher critical energy $E_{\mathrm{crit}} = 14.8AT_{\mathrm{e}}[\Sigma_{\mathrm{j}}\, n_{\mathrm{j}}\, Z_{\mathrm{j}}^2/(n_{\mathrm{e}}\, A_{\mathrm{j}})]^{2/3}$ and shorter slowing down time $\tau_{\mathrm{s}} \propto AT_{\mathrm{e}}^{3/2}/(Z^2 n_{\mathrm{e}})$ [32] as compared to protons. Here, A and Z are the mass and charge number of the resonant ion, the sum is over thermal ion species j, n_{j}, Z_{j} and A_{j} are the density, charge number and mass number of ion species j, and T_{e} and n_{e} are the electron temperature and density, respectively.

In D plasmas, the majority D ions are a natural choice for the ion species to be heated at the second harmonic ion cyclotron resonance. However, since the second harmonic deuterium resonance coincides with the fundamental hydrogen resonance, hydrogen absorption can be significant. In initially thermal plasmas which are characterised by relatively low deuteron pressures, the absorption on hydrogen often dominates, and the effects of second harmonic deuterium damping are often difficult to separate from those of the fundamental hydrogen damping. However, when the hydrogen concentration is low, or the deuteron energy density or perpendicular wave number $k_\perp$ (which increases with the plasma density) are

Table 1. ICRF frequency, $|E_+/E_-|$ ratio and perpendicular wave vector $k_\perp$ for the heating schemes studied in this paper at a magnetic field of 3.4 T. The resonant ion species are indicated in the parentheses. In the calculations of the $|E_+/E_-|$ ratio and $k_\perp$, the cold-plasma approximation has been used, the parallel wave number $k_\parallel$ is assumed to be zero and only the effect of the majority ions is considered. An electron density of 7×10^{19} m^{-3}, which is typical for the JET high-performance hybrid discharges studied in this paper, is assumed.

f (MHz)	Bulk ions	Heating scheme	$\vert E_+/E_-\vert$	$k_\perp$ (m^{-1})
51	D	$\omega = \omega_c(\mathrm{H}) = 2\omega_c(\mathrm{D})$	0.33	51
	D-T	$\omega = \omega_c(\mathrm{H}) = 2\omega_c(\mathrm{D}) = 3\omega_c(\mathrm{T})$	0.40	56
32.5	D	$\omega = \omega_c(^3\mathrm{He})$	0.11	33
	D-T	$\omega = \omega_c(^3\mathrm{He}) = 2\omega_c(\mathrm{T})$	0.17	35

high, the second harmonic deuteron absorption can become significant. This has been found to be the case in JET high performance discharges as they are characterised by relatively low hydrogen concentrations and high deuteron energy densities due to deuterium beam injection and due to a high plasma temperature and density [7, 19–25, 30, 31].

A wide variety of ICRF heating scenarios is also available for heating a D-T plasma, see e.g. [4–7, 20–24]. In addition to the scenarios discussed above for D plasmas, second harmonic heating of T becomes an option. As discussed in the introduction, second harmonic heating of T is currently envisaged as one of the standard ICRF heating scenarios for ITER at its full magnetic field. The advantage of the scenario is its applicability to 50:50 D-T plasmas. However, the wave polarisation in a D-T plasma is not particularly favourable (see table 1), which together with the absorption being a finite Larmor radius (FLR) effect tends to lead to weak absorption on the tritons in plasmas with low to moderate temperatures and densities. Another consequence of the absorption being an FLR effect is that high-energy tritons tend to interact more effectively with the wave field than tritons with low energies. This can lead to a tail on the triton distribution function with a small number of very energetic tritons. Another option for improving the ion heating is to add a few per cent of ^{3}He ions into a plasma. In this case, ^{3}He minority ions will absorb a substantial part of the ICRF power. The power absorbed by the ^{3}He ions can be efficiently transferred via collisions to the background ions, since the critical energy for ^{3}He ions is quite high ($\sim$175 keV and 195 keV in D-T and D, respectively, at typical values of $T_e = 7$ keV and $n_e = 7 \times 10^{19}$ m^{-3} in the core plasma in the discharges studied here), and the tail formed on the ^{3}He distribution function is normally moderate. It is important to note that in D-T plasmas ^{3}He ions can be present due to radioactive decay of tritium (and to a lesser extent due to D–D fusion reactions). Such residual ^{3}He minority ions can play a significant role in partition of ICRF power for second harmonic T heating, as will be shown in this paper.

The ICRF wave frequency, $|E_+/E_-|$ ratio and perpendicular wave vector $k_\perp$ are given in table 1 for the heating schemes studied in this paper. We can see that $|E_+/E_-|$ is higher for H minority heating, suggesting stronger single pass damping for H minority heating as compared to ^{3}He minority heating. For a given ICRF scheme, $|E_+/E_-|$ is higher in D-T plasmas as compared to D plasmas, suggesting better single pass absorption in D-T as compared to D plasmas. Furthermore, given its larger $|E_+/E_-|$ and perpendicular wave number $k_\perp$, hydrogen minority heating is expected to result in stronger second harmonic D damping when compared to second harmonic tritium absorption associated with ^{3}He minority heating in D-T plasmas.

3. Experimental set-up

In recent experimental campaigns on JET, good progress has been made in the development of high-performance plasma scenarios compatible with ILW. The main scenarios developed are the hybrid and baseline scenarios [9, 13, 34]. For ICRF heating studies reported in this paper, a high-performance hybrid plasma at a magnetic field of 3.3–3.4 T and a plasma current of 2.2–2.4 MA was selected as a target plasma. The hybrid scenario is an operational plasma regime designed to achieve long pulse operation with a combination of inductive and non-inductive current drive [12–14, 35, 36]. It has been proposed for ITER to allow long-pulse ($\sim$1000 s) operation at a high fusion power ($Q_{\mathrm{fus}} = P_{\mathrm{fus}}/P_{\mathrm{IN}} \geqslant 5$) at a lower plasma current than for the inductive reference baseline scenario. A hybrid target plasma was chosen mainly for two reasons. Firstly, its lower plasma current and lower engineering complexity as compared to the baseline scenario (for example the baseline scenario uses pellets for ELM control) was considered favourable to minimise operational risks. Secondly, the hybrid plasmas at JET also have lower plasma densities than baseline plasmas, which was considered favourable in terms of ICRF-acceleration of resonant ions and studies of their effects.

High-performance hybrid discharges were achieved with NBI using D and T beams combined with ICRF heating. ICRF waves were tuned either to the fundamental cyclotron frequency of minority hydrogen ions which coincides with the second harmonic cyclotron frequency of deuterium and the third harmonic cyclotron resonance of tritium, $\omega = \omega_c(\mathrm{H}) = 2\omega_c(\mathrm{D}) = 3\omega_c(\mathrm{T})$, or to the fundamental cyclotron frequency of ^{3}He ions which coincides with the second harmonic cyclotron frequency of tritium, $\omega = \omega_c(^3\mathrm{He}) = 2\omega_c(\mathrm{T})$.

The JET A2 ICRF antennas A, B, C and D [37, 38] were used for the experiments in D-T, and the A2s and the ITER-like antenna [39, 40] for experiments in D plasmas prior to DTE2. To provide ELM resilience, antennas A and B are fed via a 3 dB hybrid couplers network, while antennas C and D are fed via an external conjugate-T network or independently [41]. More information about the operation of the ICRF system

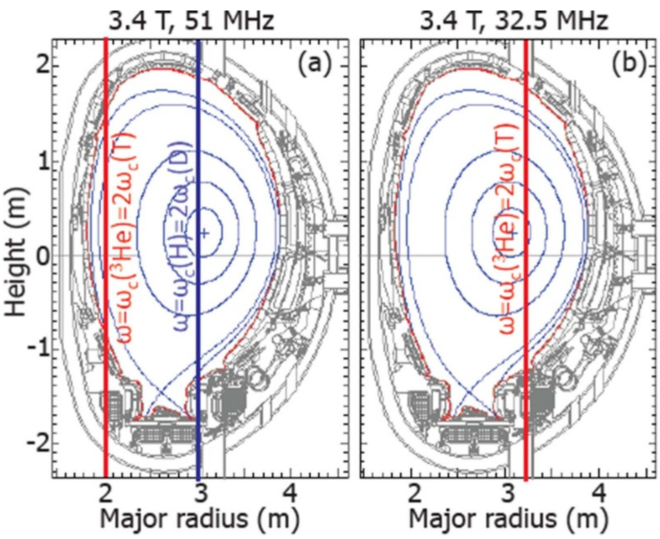

Figure 1. JET cross section for a 3.4 T/2.3 MA high-performance hybrid discharge showing the resonance positions for ICRF scenarios studied in this paper, i.e. (a) $\omega = \omega_c(\mathrm{H}) = 2\omega_c(\mathrm{D}) = 3\omega_c(\mathrm{T})$ and (b) $\omega = \omega_c(^3\mathrm{He}) = 2\omega_c(\mathrm{T})$.

during DTE2 can be found in [41]. The experiments were done with the dipole phasing, i.e. $0\pi0\pi$ phasing, with the dominant toroidal mode number of $N = 27$ corresponding to $k_{\|} = 6.7\ \mathrm{m}^{-1}$ at the antenna. This is the standard ICRH phasing used at JET. Figure 1 shows the resonance positions in the poloidal plane for the ICRF scenarios studied. The ion cyclotron resonance layers are located in the plasma core although the $\omega = \omega_c(^3\mathrm{He}) = 2\omega_c(\mathrm{T})$ resonance at 32.5 MHz is displaced from the plasma centre by about 10 cm to the low field side as compared to the $\omega = \omega_c(\mathrm{H}) = 2\omega_c(\mathrm{D})$ resonance at 51 MHz which is located virtually on-axis. For H minority heating at 51 MHz, we can also observe an inner wall $\omega = \omega_c(^3\mathrm{He}) = 2\omega_c(\mathrm{T})$ resonance in figure 1. This did not cause problems in DTE2 (T or D-T plasmas) even in the presence of tritium NBI [41].

The full energy of the D and T NBI neutrals was between 83 and 112 kV, with the power fractions of the full, half and one-third energy component depending on the injection energy [42]. Typical power fractions are ~0.5, 0.3 and 0.2, respectively, for 100 kV of D beam and ~0.6, 0.2 and 0.2, respectively, for 100 kV of T beams.

^{3}He was introduced in the machine by ^{3}He gas injection using a gas valve located in the mid-plane in feed forward (real time control of ^{3}He was not available). The ^{3}He concentration was measured by a high-resolution optical penning gauge in the sub-divertor region with an accuracy of 0.1% [12]. After discharges with ^{3}He gas injection, residual ^{3}He was measured in several subsequent discharges without ^{3}He gas injection, with the ^{3}He concentration decreasing from discharge to discharge. In addition to residual ^{3}He, an intrinsic concentration of ^{3}He of the order of 0.2%–0.4% of the electron density was measured before ^{3}He was introduced in the device. This intrinsic ^{3}He is attributed to the radioactive decay of tritium to ^{3}He during its storage.

4. Experiments in D-T plasmas

In this section, the experiments carried out in DTE2 to study second harmonic heating of T and ^{3}He minority heating are presented including comparisons with the more commonly used H minority heating/second harmonic heating of D. The section is organised as follows. First, the discharges and their objectives are discussed in section 4.1. In section 4.2, an overview of the main plasma parameters is given. The input NBI and ICRF powers are discussed in section 4.3 and the statistical analysis of the plasma performance is presented in section 4.4. Experimental evidence for fast ICRF-accelerated tritons and the discussion of their characteristics are given in section 4.5. Finally, in section 4.6 the results on ICRF + NBI modelling of the discharges are discussed including ICRF power partitioning, heating of the bulk plasma ions and electrons, and ICRF-resonant ions and their enhancements of fast ion energy content and fusion yield.

4.1. Discharges and their objectives

A total of 13 discharges were carried out with a nominal 50:50 D:T fuel mixture at a similar total gas injection rate at 3.4 T/2.3 MA. The T concentration ranged from 40% to 60%. The discharges can be divided in three groups as shown in table 2. Four discharges in group 1 were with D-T NBI and second harmonic T ICRF heating with no ^{3}He introduced in the machine. Four discharges in group 2 were carried out as those in group 1 but with ^{3}He introduced via gas injection in the vacuum vessel. In discharge 99 629, ^{3}He gas injection was introduced before the start of NBI and ICRF heating, followed by a decay of ^{3}He in high-performance phase from approximately 4% to 0.5%. Finally, five discharges in group 3 are reference pulses with D-T NBI and hydrogen minority heating/second harmonic D heating. The discharges were carried out on four experimental days over a period of more than a month with different machine conditions. In the analysis of these pulses in sections 4.3 and 4.4 below, we also include nine further discharges with H minority heating with D-T plasmas with an average T concentration of 50%–55% (discharges 99 867, 99 869, 99 910, 99 912, 99 914, 99 949, 99 950, 99 951, 99 953) carried out with an optimised [13] lower total gas injection rate.

4.2. Overview of the main plasma parameters

Figure 2 shows an overview of the main plasma parameters for three discharges, one from each group in table 2: 99 596 with H minority heating, 99 886 with second harmonic T heating, and 99 629 with ^{3}He minority heating/second harmonic T heating. Up to 28 MW of NBI power and up to 5 MW of ICRF power was applied. ICRF power modulation at 4 Hz was applied starting at $t = 9$ s and $t = 11$ s in discharge 99 629 and discharges 99 596 and 99 886, respectively, to study the ion and electron temperature responses. The core electron temperature measured with a high-resolution

Table 2. Summary of 3.4 T/2.3 MA discharges carried out in JET high performance D-T hybrid plasmas to study second harmonic heating of tritium.

Group	Objective	Pulses	Minority concentration
1	Assess second harmonic heating of T	99 597, 99 598, 99 884, 99 886	^{3}He concentration ≈ 0.2%–0.4%
2	Assess the effect of small amount of ^{3}He on second harmonic heating of T	99 629, 99 632, 99 633, 99 639	^{3}He concentration ≈ 0.5%–7%
3	Reference discharges with H minority heating/second harmonic D heating	99 594, 99 596, 99 760, 99 761, 99 767	H concentration ≈ 2%–4%

Thomson scattering system [43] and the ion temperature, measured by the impurity charge exchange diagnostic [44] utilising an injection of neon into the plasma [13], are shown at the major radius $R = 3.2$ m corresponding to the normalised toroidal flux coordinate $\rho_{tor} \approx 0.2$. They indicate that the ion temperature is higher than the electron temperature in these plasmas. The line-average core plasma density is in the range of 5×10^{19} m^{-3} in the high-performance phase, with about 10% lower density in discharge 99 629 with ^{3}He minority heating. The neutron rate and diamagnetic plasma energy content W_{DIA} with second harmonic T heating (discharge 99 886) are higher than for the other two discharges and heating schemes. Here, $W_{DIA} = W_{th} + 1.5W_{fast,\perp}$ where W_{th} is the energy content of the thermal plasma and $W_{fast,\perp}$ is the energy content of fast ions perpendicular to the background magnetic field. However, given the differences in NBI powers, it is difficult to draw general conclusions from the discharge comparison shown in figure 2 alone. In section 4.4, results from a statistical analysis of discharges in table 2 are presented for that purpose. We note that for all discharges shown in figure 2, the fusion performance deteriorates gradually in time due to impurity accumulation, which is a common feature of JET hybrid pulses in DTE2 and is addressed in detail in an accompanying publication [13].

Figure 2 also shows the ^{3}He concentration as measured by a high-resolution optical penning gauge in the sub-divertor region [12]. In discharge 99 629 with ^{3}He minority heating/second harmonic T heating, ^{3}He was puffed before the application of ICRF heating. The ^{3}He concentration was ~4% at the beginning of the ICRF heating phase and decayed to ~0.5% towards the end of the pulse.

The radial profiles of the main plasma parameters for the discharges in figure 2 are shown at $t = 8.5$ s in figure 3. The main differences between the plasma profiles are the 10% lower plasma density in discharge 99 629 with ^{3}He minority heating and the 15% higher ion temperature in discharge 99 886 with second harmonic T heating without ^{3}He gas injection. However, as can be concluded from figures 2 and 3, the overall performance of JET hybrid plasmas heated with second harmonic heating of tritium with and without ^{3}He gas injection is very similar to that with the more commonly used H minority heating/second harmonic D heating. This is because ICRH power is only a small fraction (10%–15%) of the total input power.

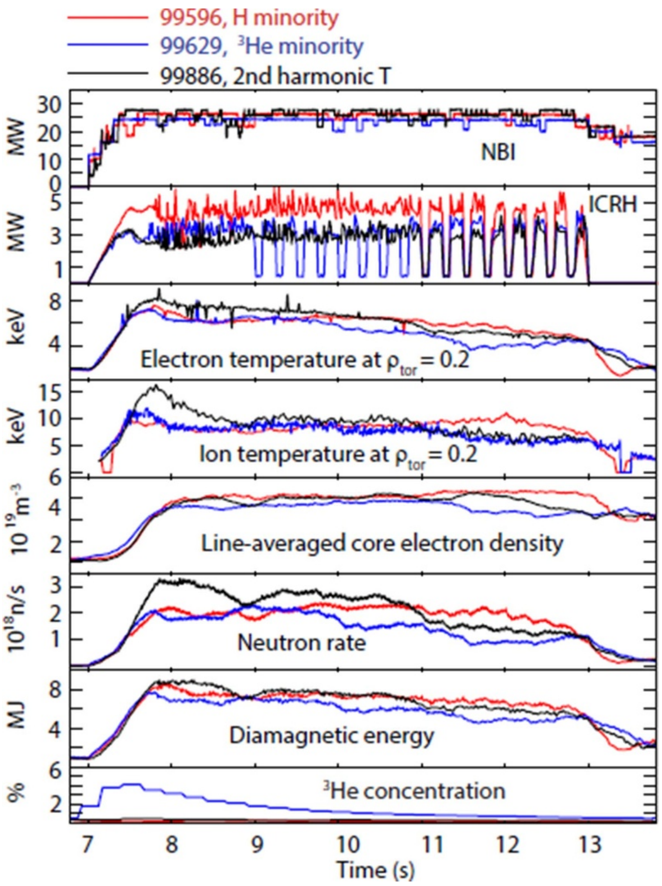

Figure 2. Overview of main plasma parameters for three JET D-T discharges with different ICRF heating schemes, i.e. discharge 99 596 with H minority heating/second harmonic D heating (red); 99 886 with second harmonic T heating (black); and 99 629 with ^{3}He minority heating/second harmonic T heating (blue): NBI and ICRH power, electron temperature the major radius $R = 3.2$ m corresponding to the normalised toroidal flux coordinate $\rho_{tor} \approx 0.2$ as given by electron cyclotron emission measurements, ion temperature at $R = 3.2$ m as measured by the impurity charge exchange diagnostic, line-averaged core electron density, neutron rate, diamagnetic energy content (constructed from magnetics measurements only) and ^{3}He concentration measured with high-resolution spectrometry in the divertor region.

4.3. Input power

During these experiments the ICRF power was limited by the antenna voltages reaching the antenna voltage limit [41].

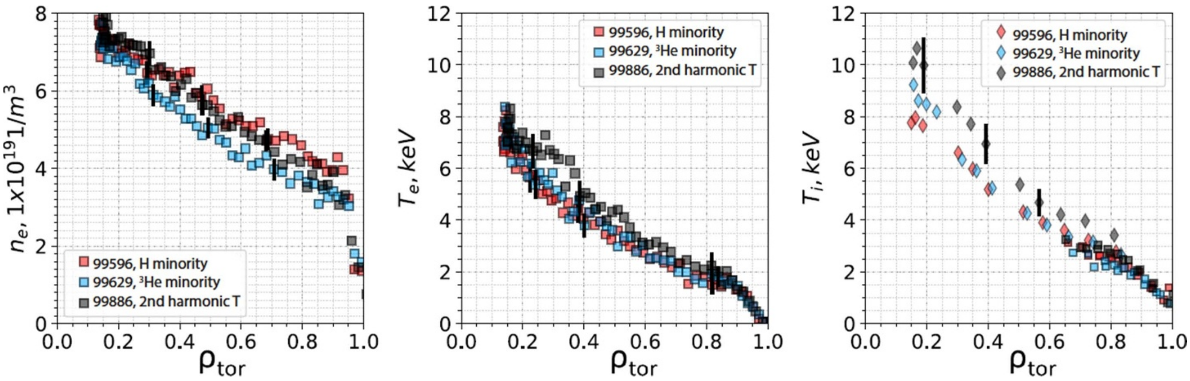

Figure 3. Radial profiles of the electron density and electron temperature as measured by the high-resolution Thomson scattering system and the ion temperature as measured by the impurity charge exchange diagnostic as the function of the normalised minor radius, i.e. the square root of the normalised toroidal flux ρ_{tor}, for the JET high performance D-T hybrid plasmas shown in figure 2 at $t = 8.5$ s (before the start of the ICRH power modulation in discharge 99 629).

Consequently, the main operational difference between the three ICRF scenarios tested was the decrease of about 35% in P_{ICRF} when reducing the ICRF frequency from 51 MHz used for H minority heating/second harmonic D heating to 32.5 MHz used for ^{3}He minority heating/second harmonic T heating. This decrease was due to a reduction in the antenna coupling resistance from about 0.6 Ω (0.8–0.9 Ω) with H minority heating/second harmonic D heating to 0.2–0.3 Ω (0.4–0.65 Ω) with second harmonic heating of T and ^{3}He minority heating for the A2 ICRF antennas A and B (antennas C and D). The lower coupling resistance at 32.5 MHz results from the combination of (a) the A2 antennas RF properties (antennas optimised at frequencies 42–51 MHz) and (b) the larger fast wave cut-off density ($n_{e,\text{ cut-off}} \sim 4 \times 10^{18}$ m^{-3} at 32.5 MHz and $\sim 2.4 \times 10^{18}$ m^{-3} at 51 MHz). With second harmonic heating of T and ^{3}He minority heating, the coupling resistance increased with the ^{3}He concentration and gas injection as shown in figure 4. The gas injection optimisation was done close to the C and D antennas and it had a stronger impact in the pulses without ^{3}He gas injection. Note that the range of gas rates was limited to stay in high performance conditions with a high core ion temperature. Injection of ^{3}He was found to have an impact on the density in the scrape-off layer (SOL) as measured by reflectometry [45]. As shown in figure 5, pulses with ^{3}He gas injection were found to have a higher SOL density and lower pedestal density. Using the measured SOL density profiles, calculations with a simplified wave coupling code [46] gave coupling resistance estimates that are broadly consistent with figure 4.

Figure 6 shows the ICRF power and NBI power as function of the total auxiliary power (NBI + ICRF power) in the experiments with different ICRF schemes in table 2. As we can see up to 3.8 and 4.5 MW of ICRF power with an ICRF frequency of 32.5 and 51 MHz, respectively, was applied. The pulses with the ICRF frequency of 32.5 MHz did not reach the same ICRF power level as the pulses with H minority heating at 51 MHz due to the ICRF coupling issues discussed above in section 4.3, which complicated their comparison. NBI power was in the range of 22–28 MW and, therefore, the dominant heating mechanism. Note that all the discharges with ^{3}He

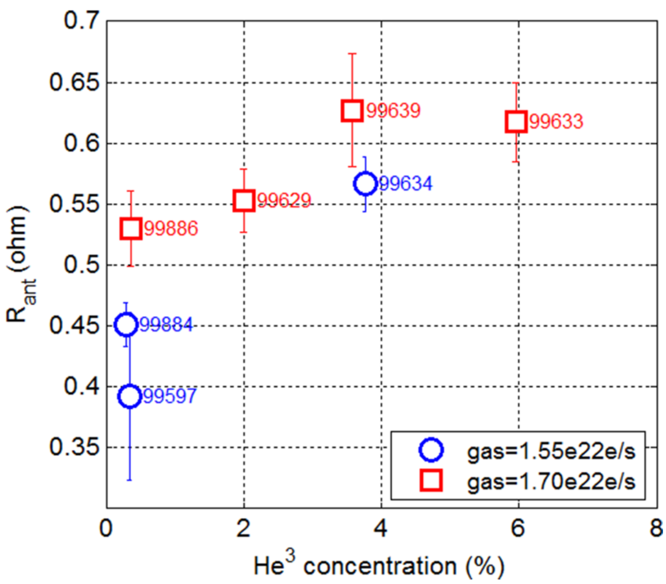

Figure 4. Antenna coupling resistance for ICRF antennas C and D as a function of ^{3}He concentration for discharges with second harmonic tritium heating with and without ^{3}He gas injection in JET high performance D-T hybrid plasmas at two levels of the total gas injection rate.

minority heating and two out of three discharges shown with second harmonic T heating had lower NBI power and lower total auxiliary power as compared with the two discharges with H minority heating in table 2. This was due to changes in the availability of neutral beam injectors between the pulses.

4.4. Plasma performance

Figure 7 shows the plasma diamagnetic energy content W_{DIA} and fusion power P_{fus} as a function of the combined NBI and ICRF heating power. Up to 35% and 5% larger P_{fus} and W_{DIA}, respectively, were obtained with second harmonic heating of T as compared to H minority heating at comparable total input powers and gas injection rates. P_{fus} and W_{DIA} with ^{3}He minority heating tend to be lower than for the other two ICRF

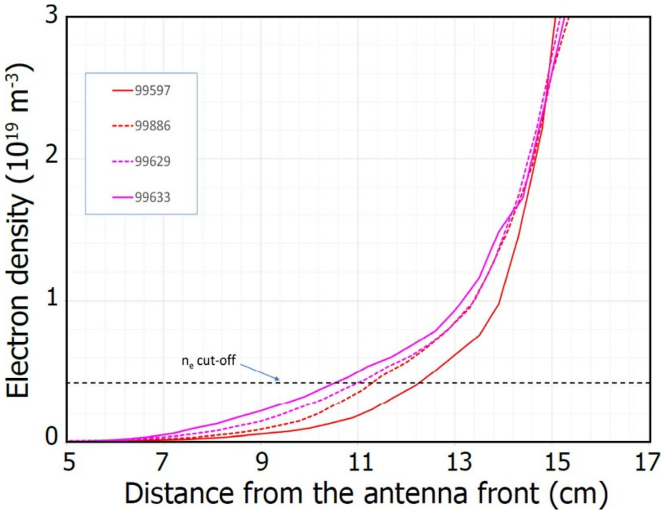

Figure 5. Electron density profiles in the scrape-off layer (SOL) as measured by reflectometry [45] for discharges 99 597 and 99 886 with second harmonic T heating without ^{3}He gas injection, and for discharges 99 629 and 99 633 with ^{3}He minority heating and ^{3}He gas injection using a midplane gas valve. The fast wave cut-off density at 32.5 MHz is also indicated.

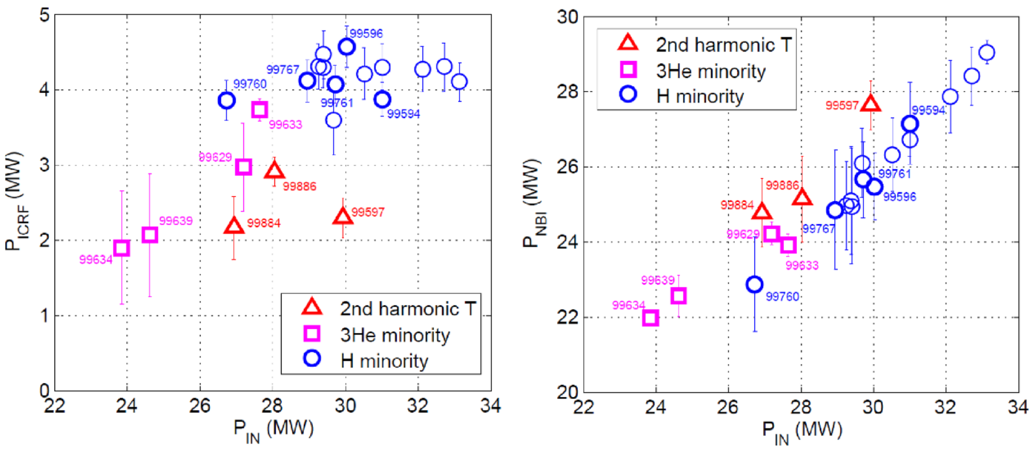

Figure 6. ICRF power (left) and NBI power (right) as function of the total auxiliary power (NBI + ICRF) in JET high performance D-T hybrid plasmas with different ICRF schemes shown in table 2. In addition, nine further discharges with H minority heating carried out with an optimised [13] lower total gas injection rate (see section 4.1) are shown with thinner blue circles. Data has been averaged over a one-second period from 8.5 to 9.5 s in each pulse. The error bars show the standard deviation of the one-second average.

schemes. Figure 8 shows the ion temperature as measured by the impurity charge exchange diagnostic at $\rho_{\text{tor}} \approx 0.2$ and the on-axis electron temperature as given by electron cyclotron emission measurements as a function of total auxiliary input power for discharges in figure 7. As we can see, the core ion temperature is up to 30% and 20% higher with second harmonic T and ^{3}He minority heating, respectively, with respect to H minority heating. The differences in the core electron temperatures are smaller than those in the ion temperatures between the different ICRF schemes. Note that discharge 99 629 with ^{3}He minority heating has almost as high ion temperature as discharge 99 884 with second harmonic T heating at the similar auxiliary power of 27 MW (see figure 8). However, discharges with ^{3}He minority heating (including 99 629) have a ∼10% lower density (see figure 3) and fuel dilution due to 2%–6% of ^{3}He, which leads to a lower fusion power as compared to second harmonic heating of T as shown in figure 7.

The above results are different from JET DTE1 ICRF-only experiments (with diagnostic T beam blips only) where higher ion and electron temperatures were observed with ^{3}He minority heating than with second harmonic heating of tritium [4–6]. The main reason for this difference between DTE1 and DTE2 experiments is the higher tail temperature of fast ICRF-accelerated tritons in DTE1 ICRF-only experiments which resulted in weaker bulk ion heating as well as broader collisional heating profiles as will be discussed in more detail later in sections 4.5 and 4.6.1.

4.5. Experimental observations of fast tritons

Experimental evidence of fast ICRF-accelerated tritons was obtained via a neutral particle analyser [47] and an upgraded magnetic proton recoil (MPRu) spectrometer [48, 49]. Figure 9 shows the time evolution of measured neutral particle fluxes of tritium at the energy of 143, 172 and 248 keV, which

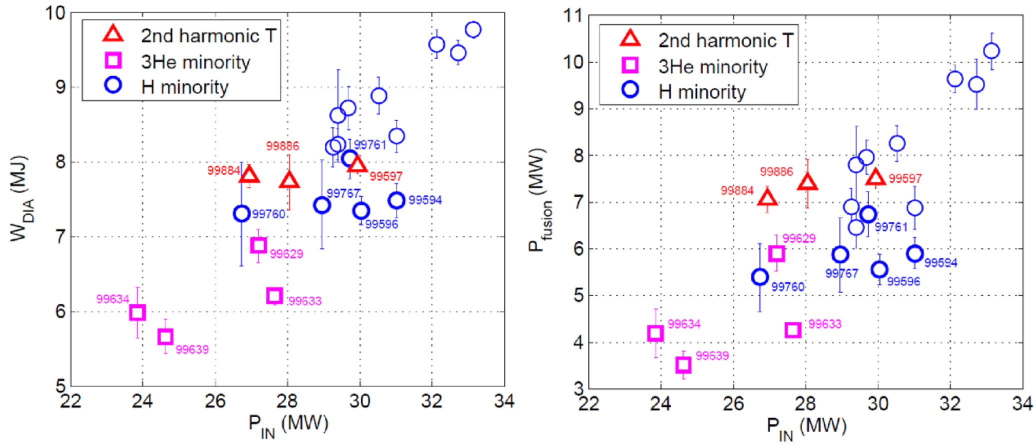

Figure 7. Plasma energy content W_{DIA} and fusion power a function of total auxiliary input power (NBI + ICRH) in JET high performance D-T hybrid plasmas with different ICRF heating schemes in table 2. In addition, nine further discharges with H minority heating carried out with an optimised [13] lower total gas injection rate (see section 4.1) are shown with thinner blue circles. Data has been averaged over a one-second period from 8.5 s to 9.5 s in each pulse. The error bars show the standard deviation of the one-second average.

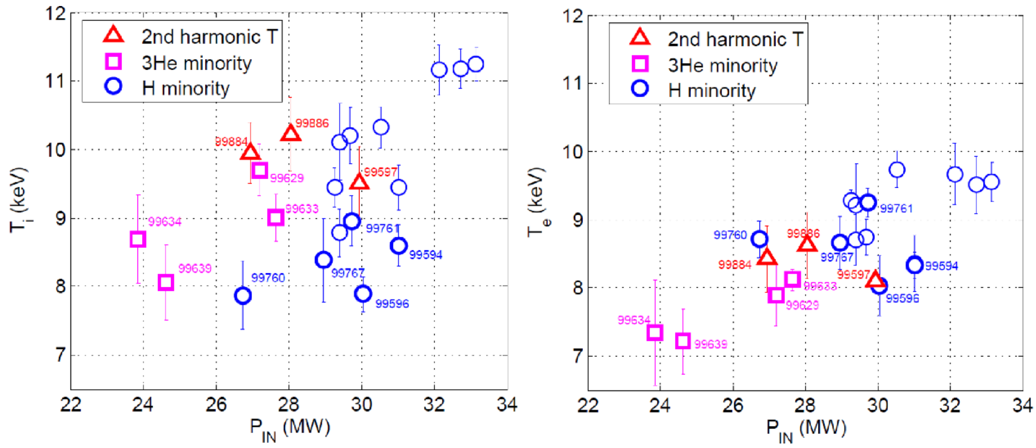

Figure 8. Ion temperature as measured by the impurity charge exchange diagnostic at $\rho_{tor} \approx 0.2$ and on-axis electron temperature as given by electron cyclotron emission measurements as a function of total auxiliary input power (NBI + ICRH) in JET high performance D-T hybrid plasmas with different ICRH schemes in table 2. In addition, nine further discharges with H minority heating carried out with an optimised [13] lower total gas injection rate (see section 4.1) are shown with thinner blue circles. Data has been averaged over a one-second period from 8.5 s to 9.5 s in each pulse. The error bars show the standard deviation of the one-second average.

are above the maximum NBI injection energy of 112 keV, for discharge 99 597 with second harmonic T heating and no ^{3}He gas injection. The measured fluxes have a maximum around $t = 7.5$ s at the start of the high-power phase and thereafter decrease throughout the main heating phase. Their time evolution follows the scaling of the fast ion energy content due to ICRF heating as given by $W_{fast} \propto P_{ICRF}\,\tau_s \propto P_{ICRF}\,T_e^{3/2}/n_e$ as shown in figure 9. The rate of change of the flux in energy decreases with increasing triton energy (from a factor of 5 when going from $E = 143$ keV to 172 keV to a factor of 2 when going from $E = 172$ keV to 248 keV) which is typical for higher harmonic heating that typically drives few resonant particles to high energies [6].

Neutral particle fluxes of tritium as the function of triton energy as measured by a neutral particle analyser [47] for discharges with different ICRH schemes are shown in figure 10. The neutral particle fluxes of tritium are strongest for second harmonic heating of T without ^{3}He gas injection, and they decrease when ^{3}He is injected for ^{3}He minority heating because less power is absorbed by tritium ions when ^{3}He is present (see section 4.6.1). The fluxes with ^{3}He gas injection are higher than those in the reference discharge with H minority heating, suggesting that some ICRF power is still absorbed on tritium during ^{3}He minority heating.

Further information about the ICRF-accelerated tritons was obtained from neutron spectroscopy measurements. The neutron spectrum from discharge 99 886 was measured with the MPRu spectrometer [48, 49], in which neutrons scatter in a thin plastic foil, producing protons that are subsequently separated in energy when passing through a magnetic field. The protons hit an array of plastic scintillators and the distribution of strike positions (X_{pos}) is closely related to the energy spectrum of the incoming neutrons. The measured MPRu spectrum for discharge 99 886 during time interval

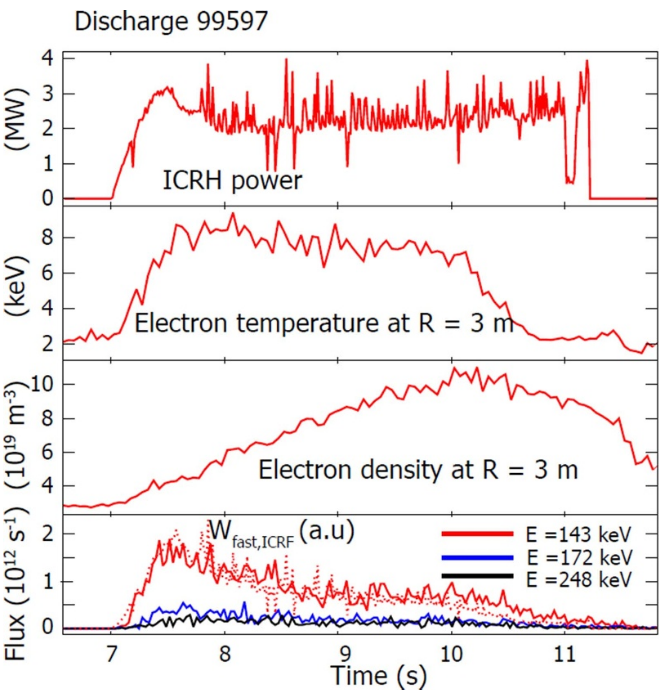

Figure 9. Time evolution of ICRF power, electron temperature T_e and electron density n_e as measured by Thomson scattering, and neutral particle fluxes of tritium at $E = 143$, 172 and 248 keV as measured by a neutral particle analyser for JET high performance D-T hybrid discharge 99 597 with second harmonic T heating and no ^{3}He gas injection. The time evolution of the estimated fast ion energy content due to ICRF heating, $W_{\mathrm{fast}} \propto P_{\mathrm{ICRF}} T_e^{3/2}/n_e$, is shown with the red dotted line in arbitrary units to compare with the flux at $E = 143$ keV.

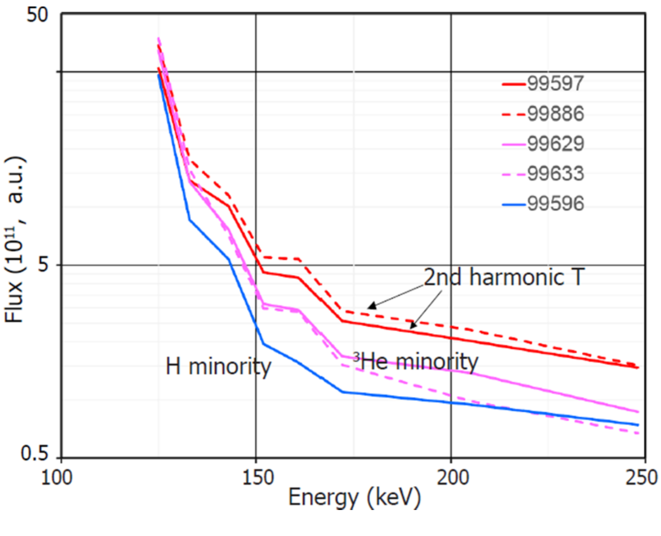

Figure 10. Neutral particle fluxes of tritium as the function of triton energy as measured by a neutral particle analyser in JET high performance D-T hybrid plasmas with different ICRH schemes. Data has been averaged over a one-second period from $t = 8$ s to $t = 9$ s in each discharge.

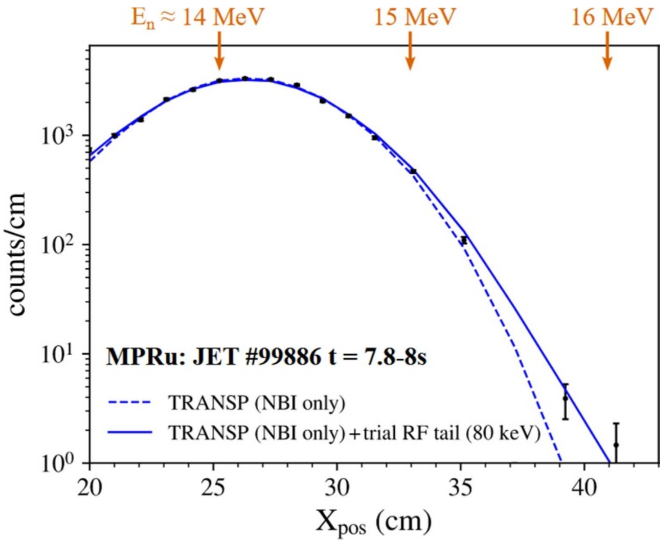

Figure 11. Neutron spectrum measured with the magnetic proton recoil spectrometer (points with error bars) for discharge 99 886 during the time interval $t = 7.8$–8 s. Also shown are comparisons with the expected spectral shapes inferred from a TRANSP simulation considering only NBI slowing down (blue dashed line) and when a trial RF tail with a tail temperature of 80 keV is added to the TRANSP distribution (blue solid line).

7.8–8 s is shown in figure 11. A TRANSP simulation, in which no ICRF-acceleration of tritium was included, was performed for the same time window, and the corresponding neutron spectral shape was computed with the DRESS synthetic neutron diagnostics code [50]. As shown in figure 11, this calculated spectrum underestimates the MPRu data on the high-energy (large X_{pos}) side of the spectrum. A number of trial distributions, representing ICRF-accelerated tritons with varying tail temperatures, were then added to the TRANSP distribution, and the corresponding neutron spectra were compared with the measurement. A trial distribution with a tail temperature of about 80 keV gave the best agreement with the MPRu data (see figure 11). From this analysis it can also be deduced that about 5% of the neutron emission is due to fusion reactions involving the ICRF-accelerated tritons. We note that the fast triton tail temperature of 80 keV is about a factor of six lower than the fast triton tail temperature of 450 keV (see figure 11 of [5]) in the plasma centre as deduced from high-energy NPA measurements in JET DTE1 ICRF-only experiments with second harmonic heating of tritium without ^{3}He gas injection. The difference in the tail temperatures of tritons arises from the differences in ICRF acceleration and collisional properties of fast tritons due to differences in input powers, plasma temperatures and densities in the two experiments. This difference is key for the understanding of the differences in their heating performance as will be discussed later in section 4.6.2.

Fast ion losses were monitored with a scintillator probe [51], which is a FILD with energy and pitch-angle resolution. No losses of fast ICRF-accelerated tritons were observed in these discharges. This was as expected due to the high plasma density of $n_e \approx 7$–8×10^{19} m^{-3} in the main heating phase (see figure 3), which limited the formation of ICRF-accelerated fast ion tails.

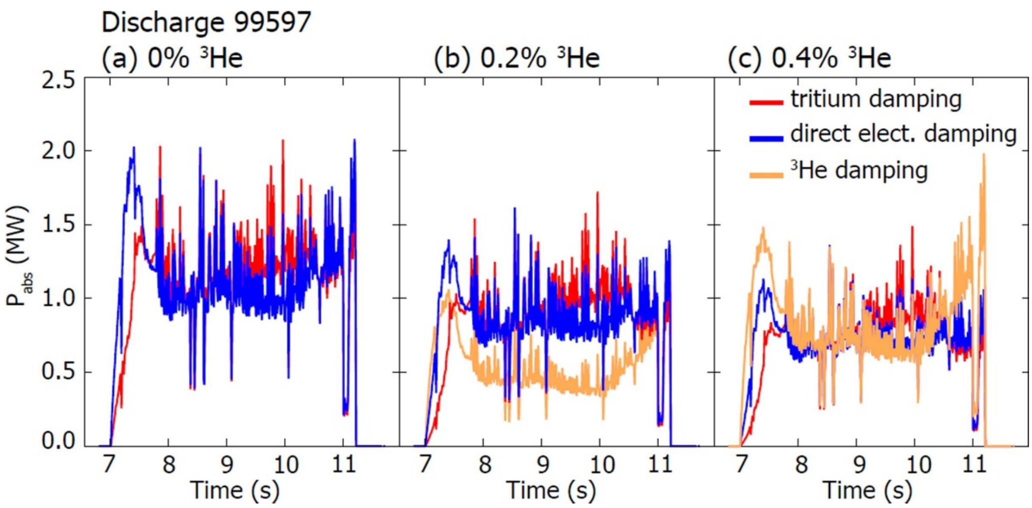

Figure 12. Time evolution of ICRF power absorption, i.e. ^{3}He damping (orange), direct electron damping (blue) and second harmonic damping of T (red), as given by PION for JET high performance D-T hybrid discharge 99 597 assuming (*a*) no ^{3}He, (*b*) a ^{3}He concentration of 0.2% and (*c*) a ^{3}He concentration of 0.4%. The input ICRF power is about 2 MW (see figure 9).

4.6. ICRF + NBI modelling

ICRF + NBI heating has been modelled with CYRANO [29]-FOPLA [52] within the heating and current drive workflow of the European Transport Solver project [53, 54], PION [26] coupled [30] with the NBI code PENCIL [55], and TORIC [27] within TRANSP [28] taking into account the NBI + ICRF synergy and using the measured data as input. In PION simulations the full toroidal mode number spectrum is included, while in CYRANO and TORIC only a single toroidal mode number $N = 27$ at the peak of the antenna spectrum is taken into account. While there is not enough experimental data on ICRF power deposition or ICRF-accelerated ions in these NBI dominated plasmas to allow contrasting the different ICRF code results against them, the main reason we have involved these different ICRF modelling codes in the present study is to document the similarities and differences between their predictions for these ITER-relevant ICRF heating scenarios on present-day experiments. This information is relevant as it provides a range of modelling results which reflects the uncertainty that arises from the differences in the ICRF codes used. It is important information to keep in mind when discussing the present results as well as when using these codes or other ICRF codes to predict the performance of these ICRF scenarios in ITER and other future fusion devices.

In the following, the results on ICRF + NBI modelling of the discharges in table 2 are discussed, including ICRF power partitioning in section 4.6.1, heating of the bulk plasma ions and electrons in section 4.6.2, and ICRF-resonant ions and their enhancements of the fast ion energy content and fusion yield in section 4.6.3.

4.6.1. ICRF power partitioning. Figure 12 shows the time evolution of the ICRF power partitioning integrated over the plasma volume for discharge 99 597 as given by PION. The input ICRF power is about 2 MW (see figure 9). Discharge 99 597 was carried out without ^{3}He gas injection. However, high-resolution optical penning gauge measurements in the sub-divertor region suggested an intrinsic concentration of ^{3}He of 0.2% of the electron density in this discharge. The measured intrinsic ^{3}He concentration in other discharges with second harmonic heating of T and no ^{3}He gas injection in these experiments was 0.4% (see table 2). Given this range of measured ^{3}He, we have carried out three PION simulations for discharge 99 597, one assuming no ^{3}He and the other ones assuming a ^{3}He concentration of 0.2% and 0.4%, respectively, to illustrate the effects of ^{3}He in the full range of ^{3}He concentrations. According to PION, a ^{3}He concentration as low as 0.2%–0.4% leads to significant changes in the ICRF power deposition as shown in figure 12. Without ^{3}He, half of the ICRF power is absorbed by electrons and the remaining half by tritons in the ICRF flat-top phase. When a ^{3}He concentration of 0.2% is added, 20%–30% of the ICRF power is absorbed by ^{3}He and the rest of the ICRF power is divided equally between electrons and tritons. When the ^{3}He concentration is increased to 0.4%, ^{3}He absorption increases further and the ICRF power is divided equally between electrons, tritons and ^{3}He. Figure 13 shows the radial ICRF power deposition profiles as given by PION for discharge 99 597 at $t = 9$ s for ^{3}He concentrations of 0%, 0.2% and 0.4%. As we can see, the power deposition is located within the plasma core within $\rho_{\mathrm{tor}} = 0.4$ and becomes slightly more peaked in the plasma centre as the ^{3}He concentration is increased.

Figure 14 shows the time evolution of the ICRF power partitioning for discharge 99 629 as given by PION. In this discharge with ^{3}He minority heating/2nd harmonic T, ^{3}He was puffed only before the application of ICRF heating. The ^{3}He concentration was ~4% at the beginning of the ICRF heating phase and decayed to ~0.5% towards the end of the pulse (see figures 2 and 14). Furthermore, ICRF power modulation was applied during a major part of the discharge for power deposition studies. According to PION, ^{3}He absorption dominates at the beginning of the ICRF phase and thereafter gradually

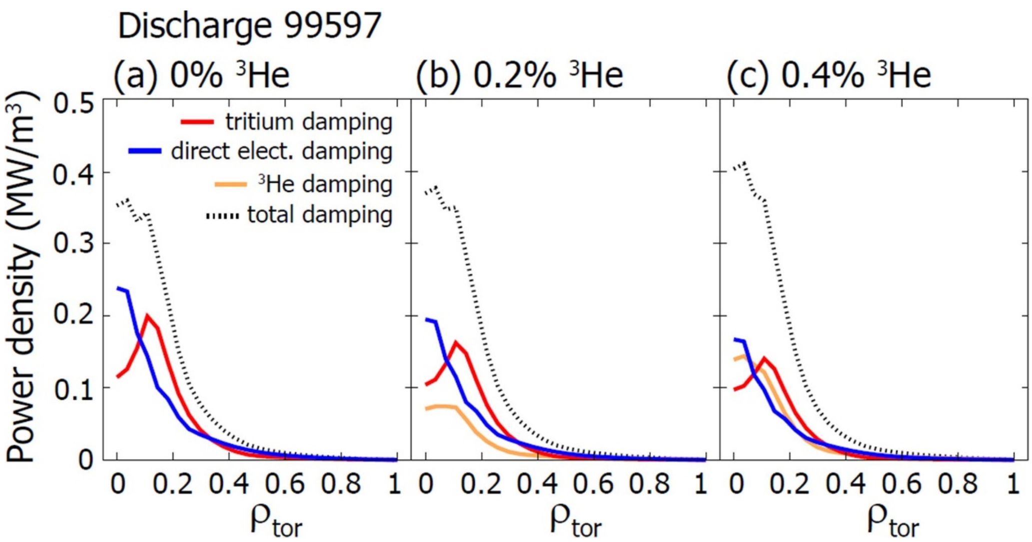

Figure 13. ICRF power partitioning as given by PION for JET high performance D-T hybrid discharge 99 597 with second harmonic heating of tritium as the function of the square root of the normalised toroidal flux $\rho_{\rm tor}$ at $t = 9.0$ s (*a*) without ^{3}He, (*b*) with a ^{3}He concentration of 0.2% and (*c*) with a ^{3}He concentration of 0.4%. The input ICRF power is about 2 MW (see figure 9).

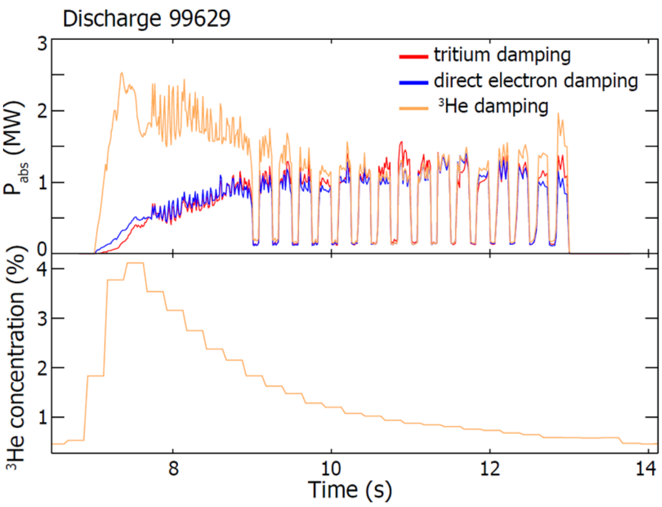

Figure 14. Time evolution of ICRF power absorption, i.e. ^{3}He damping (orange), direct electron damping (blue) and second harmonic damping of T (red), as given by PION for JET high performance D-T hybrid discharge 99 629 with ^{3}He gas injection before the application of ICRF heating followed by a decay of the ^{3}He concentration measured by a high-resolution optical penning gauge in the sub-divertor region with an accuracy of 0.1% [12]. ICRF power modulation was applied during a later part of the discharge for power deposition studies.

decreases as the ^{3}He concentration decreases in time down to 1.5%, which results in an increase in second harmonic damping of tritium and direct electron damping as shown in figure 14. Such a scheme is also envisaged for ITER, i.e. to start with a mixed ^{3}He minority/second harmonic T heating while the plasma heats up and to switch to dominant second harmonic T heating when the plasma is hot enough (see e.g. [6]). As the ^{3}He concentration decreased further from 1.5% to 0.5%, the fraction of ^{3}He absorption stayed roughly constant according to PION (see figure 14), illustrating once more that even small amounts of ^{3}He can absorb considerable amount of power in this scenario.

Similar results as those above with PION have been obtained with modelling using TORIC within TRANSP and CYRANO. Table 3 summarises the modelled ICRF power partitioning for selected discharges from table 2 as given by the three codes. While there are significant differences in the numerical methods and physics models used (e.g. with respect to D damping included in CYRANO, see table 3), the results are broadly consistent with each other for ^{3}He concentrations of 3%–5%. For low ^{3}He concentration of 0.3%–0.4%, CYRANO gives lower direct electron absorption by electron Landau damping (ELD) and transit time magnetic pumping (TTMP), possibly because it includes the fundamental D absorption located at mid-radius at the HFS of the plasma. The ^{3}He absorption as given by CYRANO is also slightly smaller than given by PION and TORIC in these conditions. Furthermore, we note that wave damping by T beam ions accounts for approximately 10% and less than 5% of ICRF power for ^{3}He concentrations of 0.3%–0.4% and 3%–5%, respectively, in these JET D-T discharges according to all codes used. In ITER, there will be no tritium beams and, therefore, no wave damping by T beam ions.

4.6.2. Heating of the bulk plasma electrons and ions. Figure 15 shows the total radial NBI + ICRF heating profiles of bulk ions and electrons as given by PION for discharge 99 597 with second harmonic heating of tritium as the function of the square root of the normalised toroidal flux at $t = 9.0$ s. Results from three PION simulations assuming a ^{3}He concentration of 0%, 0.2% and 0.4%. Also, results from NBI-only simulation using the measured plasma parameters as the input are shown. As we can see, adding ICRF power in discharge 99 597 increased the collisional ion heating in the plasma core. There was also an increase in bulk

Table 3. Modelled ICRF power partitioning at selected times in JET high performance D-T hybrid discharges from table 2 with different ^{3}He concentrations. In each table element, the value is quoted in the following order: CYRANO, TORIC within TRANSP, and PION, with a slash between them. In PION the full toroidal mode number spectrum is included while in CYRANO and TORIC only a single toroidal mode number $N = 27$ at the peak of the antenna spectrum is taken into account.

Discharge, time and ^{3}He concentration	Electrons (%)	Total deuterium (%)	Total tritium (%)	^{3}He (%)
99 597 at $t = 8.95$ s; 0% ^{3}He	16/36/49	18/–/–	66/64/51	0/0/0
99 886 at $t = 9.1$ s; 0.4% ^{3}He	15/28/30	12/–/–	48/37/35	25/34/35
99 884 at $t = 8.9$ s; 0.3%–0.4% ^{3}He	18/29/36	16/–/–	46/41/31	20/30/33
99 633 at $t = 9.1$ s; 5% ^{3}He	6/8/13	4/–/–	7/8/9	83/85/78
99 639 at $t = 8.9$ s; 3% ^{3}He	6/9/12.5	8/–/–	11/11/6.5	75/80/81

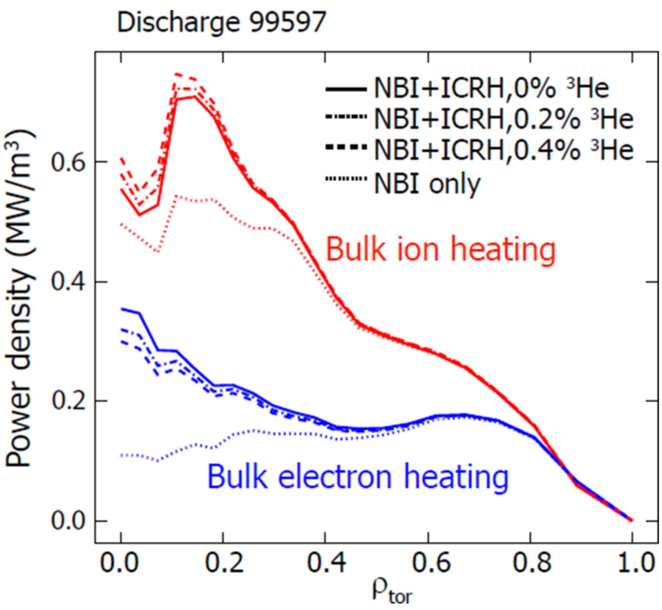

Figure 15. Collisional bulk ion heating (red) and bulk electron heating (which is the sum of collisional electron heating and direct electron damping of the launched ICRF waves via electron Landau damping and transit time magnetic pumping) (blue) power density as given by PION for JET high performance D-T hybrid discharge 99 597 with second harmonic heating of tritium as the function of the square root of the normalised toroidal flux ρ_{tor} at $t = 9.0$ s without ^{3}He (solid lines) and with a ^{3}He concentration of 0.2% (dash-dotted lines) and 0.4% (dashed lines). The dotted lines indicate the results for NBI-only simulation using the measured plasma parameters as the input. The input NBI and ICRF power is about 27.5 MW and 2 MW, respectively.

electron heating due to ICRF heating. Bulk electron heating by ICRF heating arises in this scenario via two mechanisms: (1) direct electron damping of the launched ICRF wave via ELD and TTMP and (2) collisional electron heating by ICRF-accelerated ions, i.e. tritons and ^{3}He minority ions. For the ^{3}He concentration of 0.4%, the fraction of ICRF power going to collisional electron heating and direct electron damping as given by PION are 11% and 32%, respectively, while the remaining 57% of the ICRF power goes to collisional bulk ion heating. When no ^{3}He is considered in the PION simulations, these fractions change to 10%, 47% and 43%, respectively. Despite the significantly lower input ICRF power of 2.3 MW as compared to the input NBI power of 27.5 MW in this discharge, ICRF heating resulted in a $\sim$10%–20% and $\sim$155%–210% increase in the on-axis bulk ion and electron heating, respectively, according to PION. Break-in-slope and fast Fourier transform analysis of ion and electron temperature in response to ICRH power modulation (see figure 2) corroborated the central ICRH power deposition of bulk plasma ions and electrons in these experiments. For all the discharges modelled using the three codes CYRANO, TORIC and PION (see table 3), PION gave somewhat higher direct electron damping as compared to CYRANO and TORIC. This means that bulk ion/electron heating due to ICRH as given by CYRANO and TRANSP would have been somewhat larger/smaller than those given by PION shown in figure 15.

It is important to note that the bulk ion and electron heating fractions by ICRF heating given above for discharge 99 597 are significantly different from those in JET DTE1 ICRF-only discharges with second harmonic heating of tritium. In the DTE1 plasma conditions, the bulk ion and electron heating fraction as given by PION was $\sim$10% and $\sim$90%, respectively (see figure 13 in [6]). The main reason for this difference is the factor of six higher tail temperature of ICRF-accelerated fast tritons in DTE1 experiments as discussed in section 4.5. Due to their high energy well above the critical energy, the fast tritons mainly heated the plasma electrons via collisions in DTE1 plasmas while in DTE2 their energy was lower, which resulted in stronger collisional bulk ion heating.

Figure 16 shows the bulk ion and electron heating due to ICRH as given by PION for discharge 99 629 with ^{3}He minority heating. The bulk ion heating due to ICRH takes place via collisions between bulk ions and ICRF-accelerated ions while the bulk electron heating due to ICRH takes place via two mechanisms, i.e. collisional electron heating and direct electron damping of the launched wave. The bulk ion and electron heating due to ICRH have been calculated as a difference between two PION runs, one with and another one without ICRF heating, using the measured plasma parameters as input in both runs. In discharge 99 629 the ^{3}He concentration decreased from 4% down to 0.5% throughout the ICRF heating phase and ICRH power modulation was added from $t = 9$ s onwards (see figures 2, 9 and 14). As we can see figure 16, bulk ion heating by ICRH exceeded bulk electron heating by ICRH according to PION throughout the heating phase although the difference became very small in the transient phases of ICRH power modulation and ICRF power switch off.

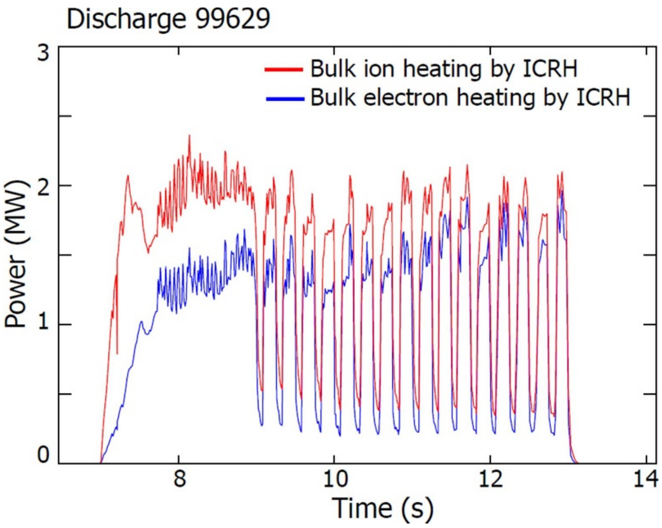

Figure 16. Collisional bulk ion heating due to ICRH (red) and bulk electron heating due to ICRH (blue) as given by PION for JET high performance D-T hybrid discharge 99 629 with ^{3}He minority heating and a decay of ^{3}He concentration (see figures 2 and 14).

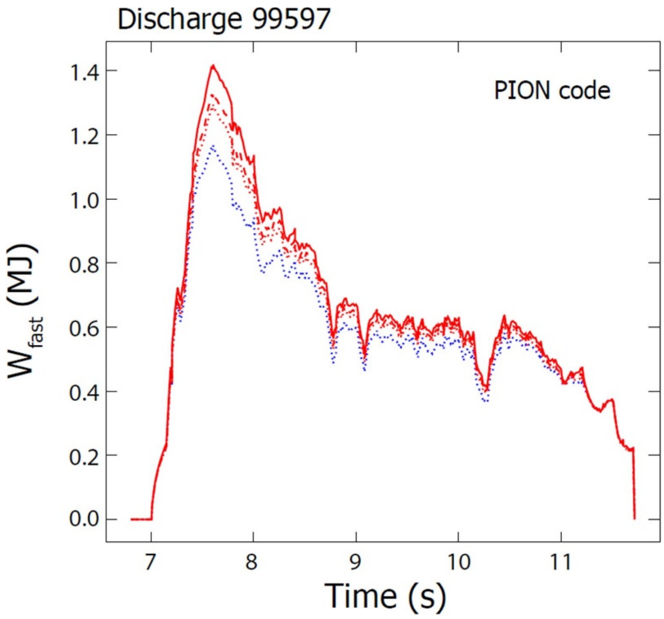

Figure 17. Fast triton energy content as given by PION assuming a ^{3}He concentration of 0% (red solid line), 0.2% (red dashed line) and 0.4% (red dotted line) for JET high performance D-T hybrid discharge 99 597 with second harmonic heating of tritium and no ^{3}He gas injection. For reference, the fast triton energy content due to NBI only is also shown (blue dotted line).

4.6.3. Modelling of ICRF-resonant ions. Figure 17 shows the fast triton energy content $W_{\text{fast, T}} = W_{\text{tot, T}} - W_{\text{th, T}}$ as given by PION for discharge 99 597 with second harmonic heating of tritium and no ^{3}He gas injection. Results from three PION simulations assuming a ^{3}He concentration of 0%, 0.2% and 0.4% are shown and compared with the fast triton energy content due to NBI only. As can be seen in figure 17, the enhancement of $W_{\text{fast,T}}$ due to ICRF-accelerated ions as given by PION has a maximum in the early phase of the discharge around $t = 7.5$ s and thereafter decays in time. This time behaviour is similar to that of the measured neutral particle fluxes of tritium above the maximum NBI injection energy shown in figure 9. When the ^{3}He concentration was increased from 0% to 0.2% (0.4%) in the simulations, the enhancement of $W_{\text{fast,T}}$ due to ICRF-accelerated tritons decreased by about 25%–35% (40%–50%). This decrease in $\text{W}_{\text{fast,T}}$ is due to a decrease in the absorbed ICRF power on tritium by about 20%–30% (30%–40%) as shown in figure 12. From these results we conclude that the enhancement of $\text{W}_{\text{fast,T}}$ due to ICRF-accelerated tritons decreases roughly linearly with the absorbed ICRF power on tritium, as expected.

The enhancement of the fast ion energy content W_{fast} due to ICRF-accelerated ions (i.e. T and ^{3}He ions for ^{3}He minority heating/second harmonic T heating and H and D ions for H minority heating/second harmonic heating of D) as given by PION for JET high performance D-T hybrid discharges with different ICRF schemes in table 2 at $t = 9$ s are shown in figure 18. Here, a ^{3}He concentration of 0.4% in discharges with second harmonic T heating is assumed. As we can see, W_{fast} due to ICRF-accelerated ions was about 0.25 MJ for H minority heating and a factor of two smaller for second harmonic heating of T and ^{3}He minority heating. We estimate that W_{fast} due to ICRF-accelerated ions contributed only up to 5% to W_{DIA} shown in figure 7. Here, we have used the fact that W_{fast} due to ICRF-accelerated ions is mainly perpendicular to the background magnetic field and the fact that the diamagnetic energy content is given by $W_{\text{DIA}} = W_{\text{th}} + 1.5W_{\text{fast},\perp}$, as discussed above in section 4.2.

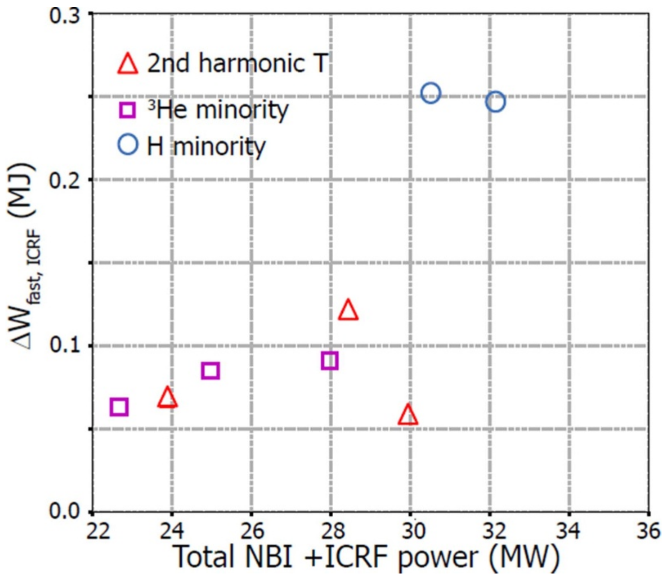

Figure 18. Enhancement of the fast ion energy content W_{fast} due to ICRF-accelerated ions (i.e. T and ^{3}He ions for ^{3}He minority heating/second harmonic T heating, and H and D ions for H minority heating/second harmonic heating of D) as given by PION for JET high performance D-T hybrid discharges with different ICRF schemes in table 2 at $t = 9$ s. A ^{3}He concentration of 0.4% in discharges with second harmonic T heating is assumed.

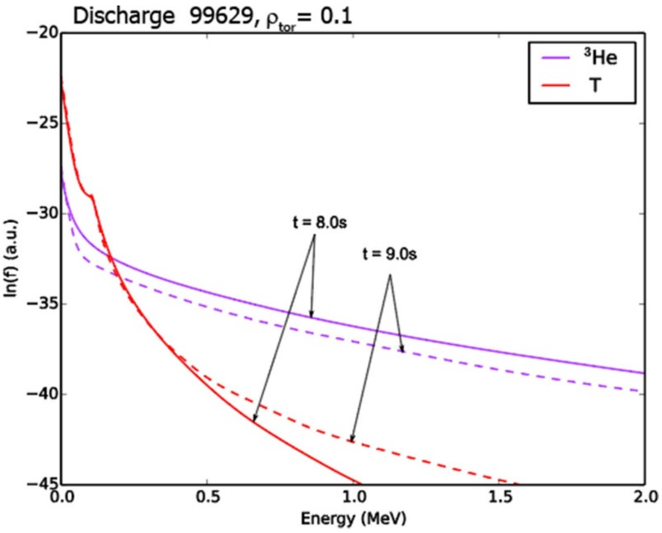

Figure 19. Distribution functions of tritons and ^{3}He at $\rho_{tor} = 0.1$ as calculated by PION for JET high performance D-T hybrid discharge 99 629 at $t = 8$ s and 9 s with a ^{3}He concentration of 3% and 1.5%, respectively. The ICRF power density absorbed by ^{3}He is 0.38 and 0.18 MW m^{-3} and the ICRF power density absorbed by T is 0.09 and 0.16 MW m^{-3} at $t = 8$ and 9 s, respectively.

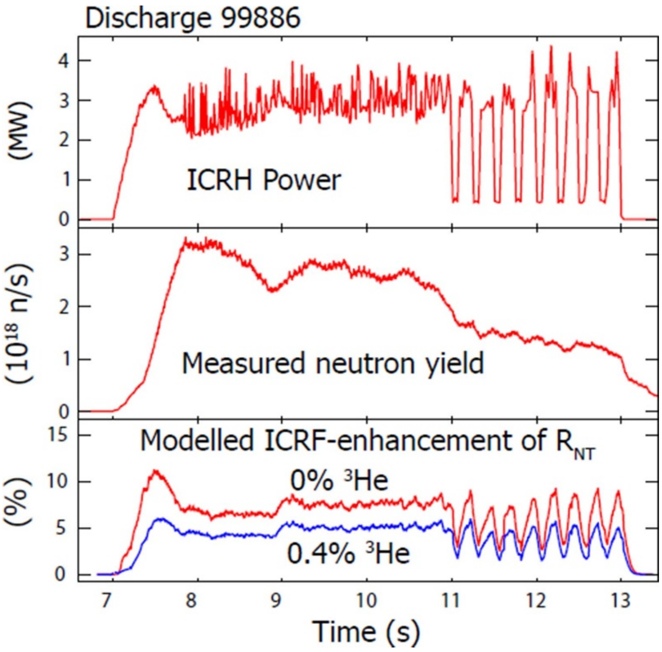

Figure 20. ICRH power, measured neutron rate R_{NT}, and modelled enhancement of R_{NT} due to ICRF-accelerated tritons as given by PION for JET high performance D-T hybrid discharge 99 886 assuming a ^{3}He concentration of 0% (red) and 0.4% (blue).

In figure 19 the modelled distributions functions of ^{3}He ions and tritons as given by PION are shown at $t = 8$ s and $t = 9$ s in discharge 99 629 with a ^{3}He concentration of 3% and 1.5%, respectively, during the ^{3}He scan. The decrease in the ^{3}He concentration results in a decrease in the magnitude of the ^{3}He fast ion tail as well as an increase in the fast T tail.

The modelled ICRF-enhancement of the D-T neutron yield due to ICRF-accelerated tritons as given by PION for discharge 99 886 with second harmonic T heating without ^{3}He gas injection is shown in figure 20 assuming a ^{3}He concentration of 0% and 0.4%. It has been calculated as a difference between two simulations for each assumed ^{3}He concentration, one with and one without ICRF power, using the measured plasma parameters as input. The ICRF enhancement is below 10% and decreases as the ^{3}He concentration is increased from 0% to 0.4% in the simulations. In the time interval of $t = 7.8$ s–8 s, the ICRF enhancement is 7% and 4%–5% with the ^{3}He concentration of 0% and 0.4%, respectively. The latter range agrees with the ICRF enhancement of about 5% as measured with the MPRu spectrometer (see section 4.5). At $t = 8$ s, the computed tail temperature and density of fast tritons at the resonance are 75 keV and 5.3×10^{18} m^{-3}, and 70 keV and 4.7×10^{18} m^{-3}, for the ^{3}He concentration of 0% and 0.4%, respectively. They do not change more when the ^{3}He concentration is varied in this range because the change in the ICRF power density absorbed by tritons at the resonance is not very large (see figure 13). The computed tail temperatures agree well with the experimental estimate of about 80 keV as given by the MPRu spectrometer.

The enhancement of P_{fus} due to ICRF-accelerated tritons and deuterons is shown in figure 21 for the discharges in table 2. It has been calculated as a difference between two simulations for each discharge, one with and one without ICRF power, using the measured plasma parameters as input. An intrinsic ^{3}He concentration of 0.4% has been used for discharges with second harmonic T heating without ^{3}He gas injection. As we can see from figure 21, the enhancement of P_{fus} due to ICRF-accelerated ions in these D-T plasmas is 5%–7% for H minority heating/second harmonic D heating, 2%–5% for second harmonic T heating and 1%–3.5% for ^{3}He minority heating. Among the discharges with second harmonic T heating, enhancements in P_{fus} and W_{fast} (see figure 18) as given by PION were smallest in discharge 99 597 with the highest total input power of 30 MW. The reason is that in this discharge the ICRF power per tritium beam particle was smallest and the plasma density was largest, which reduced the enhancement of the fast T tail as compared to other two discharges (99 884 and 99 886) with second harmonic T heating. The enhancements in P_{fus} by ICRF-accelerated ion agree well with earlier modelling predictions, see e.g. [21], and are smaller than the enhancement of D–D fusion yield of 5%–30% due to ICRF-accelerated deuterons found earlier in JET D hybrid plasmas with D NBI and H minority heating/second harmonic D heating [19, 21–25]. The enhancement in D-T due to ICRF-accelerated ions is lower because the D–D and D-T fusion cross sections peak at different energy regions. While D–D fusion cross section increases up to its maximum which is in the MeV range, the D-T fusion cross section peaks around 120 keV and decreases rapidly beyond this energy. Since the beam energy at JET is close to the optimal energy for D-T fusion reactions to occur and it is often the resonant beam ions that are efficiently accelerated by ICRF waves, a lower enhancement due to ICRF-accelerated ions is obtained in D-T as compared to D plasmas.

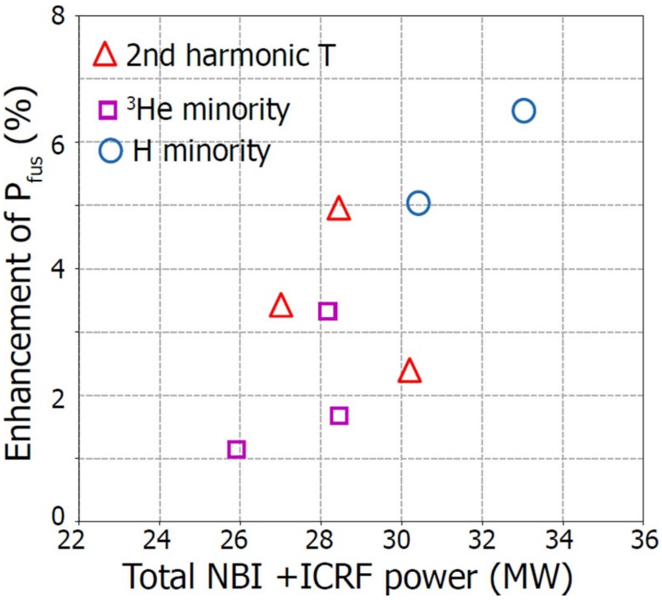

Figure 21. Calculated enhancement of P_{fus} due to ICRF-accelerated tritons and deuterons as given by PION for JET high performance D-T hybrid plasmas in table 2 at $t = 9$ s. A ^{3}He concentration of 0.4% in discharges with second harmonic T heating is assumed.

According to PENCIL, the thermal fraction of P_{fus} is about 25%–30%, 30%–35% and 35%–45% for ^{3}He minority heating, H minority heating and second harmonic T heating, respectively. These thermal fractions are similar to the thermal fusion fraction of 40% found in the best performing JET high-performance hybrid DTE2 discharge with higher input power of 33 MW (29 MW of NBI and 4 MW of ICRF power tuned to a H minority resonance) [13]. The thermal contribution of P_{fus} for second harmonic T heating is largest due to its highest ion temperature (see figure 8) and the absence of fuel dilution by injected ^{3}He which decreases the fusion performance for ^{3}He minority heating (which also has a 10% lower density, see figure 3). We conclude that the large thermal contribution of P_{fus} for second harmonic T heating is the main reason for its high P_{fus} (see figure 7).

5. Experiments to study ^{3}He minority heating in deuterium plasmas

Prior to DTE2, experiments with ^{3}He minority heating with D as the main ion species were carried out in JET high-performance hybrid discharges at a magnetic field of 3.3 T and a plasma current of 2.2 MA in similar conditions to those in the DTE2 experiments discussed in section 4. These experiments are included in this paper because their results guided the preparation of the DTE2 experiments we report e.g. by identifying the ^{3}He minority concentration range of interest to explore in D-T. This was relevant since it reduced the experimental time required in D-T. Their results also support our conclusions from the DTE2 experiments. The objective of the experiments in D plasmas was to study the effects of the ^{3}He concentration on the plasma performance during ^{3}He minority heating and to compare this ICRF heating scheme with the more commonly used H minority heating/second harmonic D heating. A summary of the discharges is given in table 4. There are two groups of discharges. In group 1, 3–5 MW of ICRF power with an ICRF frequency of 32.5 MHz was applied while NBI power was in the range of 19–25 MW. The ^{3}He concentration was increased gradually from 0% up to 8% of the electron density from discharge to discharge. The discharges in group 2 were carried out with the more commonly used H minority heating/second harmonic D heating in similar plasma conditions as those in group 1 for comparison.

Figure 22 shows the ICRF and NBI power as a function of the ^{3}He concentration for the discharges in table 4 as well as for eight further hybrid discharges with H minority heating (94 627, 94 632, 94 633, 94 634, 94 635, 94 636, 94 644, 94 645) in similar conditions but with a wider range of the NBI powers. As we can see, ICRF power was in the range of 3–5 MW while NBI power was in the range of 20–25 MW. Figure 23 shows the variation of the neutron rate and plasma diamagnetic energy content as a function of ^{3}He minority concentration for discharges in figure 22. As we can see in figure 23, the highest neutron rates with ^{3}He minority heating and H minority heating are similar even though the best discharges with H minority heating have about 2 MW more NBI power. Most importantly, there is a difference in the thermal and non-thermal neutron rates measured with these two heating schemes given the fact that the neutron rate with H minority heating in deuterium plasmas can be enhanced by 5%–30% by ICRF-acceleration of NBI-injected deuterons [19, 21–25] which does not take place with ^{3}He minority heating. The highest neutron rates with ^{3}He minority heating are obtained at low ^{3}He concentrations of ~2%, which also coincides with the highest plasma energy content. Given these results, the DTE2 experiments with ^{3}He minority heating were carried out with ^{3}He concentration of 2%–4% as discussed in section 4.1. In D plasmas, it was also experimentally verified in this series of experiments (not shown) that adding ~2% of ^{3}He in a hybrid D plasma heated by a combination of deuterium NBI and H minority ICRF heating/2nd harmonic D heating has virtually no effect on its fusion performance, impurity behaviour, pedestal and ELMs. These results are encouraging for ITER since a low ^{3}He concentration when using ^{3}He minority heating in ITER would reduce not only fuel dilution by ^{3}He but also ^{3}He consumption and, thereby, the operational cost. The results are also well in line with earlier computational work [56–59] for ITER where good absorption performance with a ^{3}He concentration of ~3% was found. It should also be noted that prior to the experiments reported in this paper, a ^{3}He concentration in the range of ~5% was considered necessary for ITER to achieve the best ion heating based on earlier experimental and modelling work. The results in figure 23 show, however, that this is probably not the optimum ^{3}He concentration for high-performance plasmas. The role of ^{3}He in the observed plasma performance is being analysed and will be reported elsewhere.

Table 4. Summary of 3.3 T/2.2 MA discharges carried out in JET high performance D hybrid plasmas to study ^{3}He minority heating with pulse-to-pulse variation of the ^{3}He concentration.

Group	Objective	Pulses	Minority concentration
1	^{3}He minority heating with a scan in the ^{3}He concentration	94 670–94 681	^{3}He concentration varied from 1.5% to 8% from pulse to pulse
2	Discharges with H minority heating	94 665–94 669	H concentration = 6%–7%

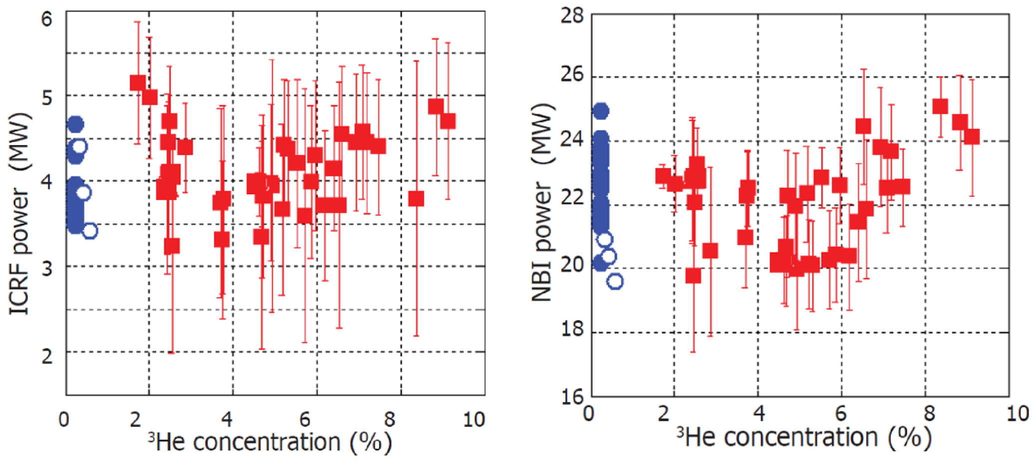

Figure 22. ICRF power and NBI power in JET high performance D hybrid discharges with ^{3}He minority heating (red) and in those with H minority heating (blue). Data is averaged over 0.4 s time intervals between $t = 7.8$ s and $t = 9$ s. Blue open circles show pulses with H minority heating in group 2 in table 4 while blue filled circles indicate H minority heating in other D hybrid discharges in similar plasma conditions and with a wider range of NBI powers. The error bars show the standard deviation of the average.

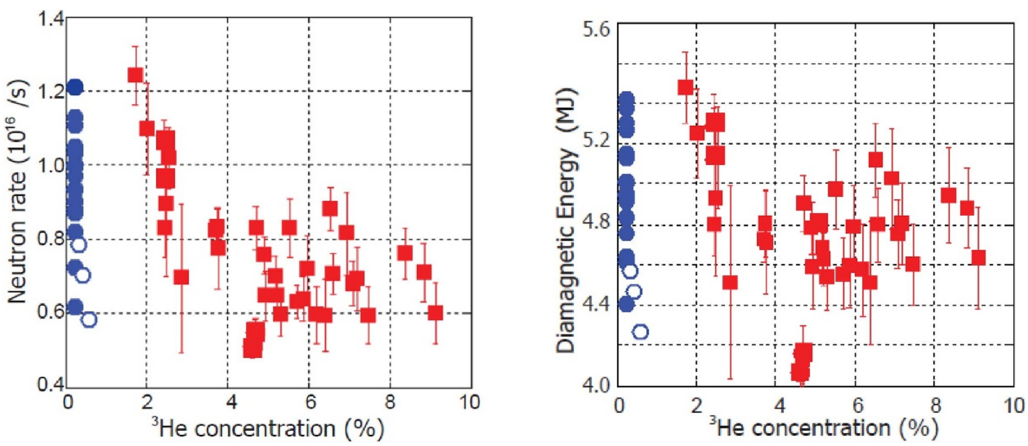

Figure 23. Neutron rate and plasma diamagnetic energy content as a function of ^{3}He minority concentration for JET high performance D hybrid discharges shown in figure 22. The colours, legends and error bars are as in figure 22.

6. Discussion and conclusions

The main difficulties encountered in the experiments to study the reference ICRF heating schemes for ITER D-T plasmas, i.e. second harmonic T heating and ^{3}He minority heating, in DTE2 hybrid plasmas reported in this paper were the low ICRF power at 32.5 MHz and low NBI as compared to other high performance hybrid discharges in DTE2. The low ICRF power was partly due to the lower coupling resistance of the A2 antennas at 32.5 Hz (which should not become an issue for these scenarios in ITER as they will use frequencies in the range of 50 MHz) and the unavailability of the ITER like ICRF antenna during DTE2 [41]. Due to the differences in ICRF and NBI powers, it was very difficult to find adequate plasma engineering matches to compare ^{3}He minority heating/second harmonic T heating with the more standard H minority heating/second harmonic D heating. Nevertheless, it was possible to successfully integrate and characterise them in JET high-performance hybrid discharges with D and T as the main ion species. Apart from issues related to antenna coupling mentioned above, there were no problems, e.g., related to enhanced plasma–wall interaction, during their use in DTE2. Overall, second harmonic heating of T was found to perform favourably as compared to the commonly used H minority heating as well as ^{3}He minority heating. In particular, up to 35% and 5% larger fusion power and plasma diamagnetic energy content, respectively, were obtained with second harmonic heating of T as compared to H minority heating at comparable total input powers and gas injection rates. Furthermore, the core ion temperature was up to 30% and 20% higher with second harmonic T and ^{3}He minority heating, respectively, with respect to H minority heating. According to NBI + ICRF modelling by PION, this was thanks to a 10%–20% increase in on-axis bulk ion heating by ICRF heating added to NBI in these D-T plasmas (although the ICRF power was significantly lower than the NBI power) due to its central localisation in the region of the wave-particle resonance which can be externally controlled by the choice of the ICRF wave frequency and the applied magnetic field. Central power deposition was confirmed with the break-in-slope and fast Fourier transform analysis of the ion and electron temperatures in response to ICRF power modulation. The tail temperature of fast ICRF-accelerated tritons, their enhancement of the fusion yield and time behaviour as measured by an MPRu spectrometer and neutral particle analyser were found in agreement with PION modelling. No losses of ICRF-accelerated ions were observed by fast ion detectors, which was as expected given the high plasma density of $n_e \approx 7\text{–}8 \times 10^{19}$ m^{-3} in the main heating phase that limited the formation of ICRF-accelerated fast ion tails. An intrinsic concentration of ^{3}He ions of the order of 0.2%–0.4% of the electron density was measured in D-T plasmas and attributed to radioactive decay of T to ^{3}He. According to modelling, even such low levels of ^{3}He lead to absorption of up to ∼30% of the ICRF power by ^{3}He ions. We also successfully demonstrated an ITER relevant NBI + ICRF heating scheme in high-performance hybrid plasmas where the plasma was first heated up with dominant ^{3}He minority heating and, thereafter, ^{3}He minority heating was reduced and T and direct electron absorption increased by letting the ^{3}He concentration decay during the main heating phase. However, according to NBI + ICRF modelling, the ion temperatures in the range of 10 keV in these hybrid discharges were not high enough for second harmonic T damping to become the dominant absorption mechanism. In such conditions using small amounts of ^{3}He minority ions can provide an additional means to optimise this ICRF scenario. This may also become relevant e.g. in the plasma ramp up phase in ITER when the plasma is not yet hot enough for efficient bulk ion heating by second harmonic T damping. Bulk ion heating by second harmonic T damping is one of the unique properties of ICRF heating in ITER. In fact, it is foreseen that ICRF heating will be the only scheme among the auxiliary heating schemes envisaged in ITER that can provide dominant bulk ion heating. The other heating methods in ITER, i.e. heating with electron cyclotron waves and NBI using MeV-energy-range ions, will provide mainly electron heating.

Our results are in contrast with earlier JET DTE1 ICRF-only H-mode results where second harmonic heating of tritium yielded poorer ICRF heating performance with respect to ^{3}He minority heating. The main reason for the better ICRF heating performance of second harmonic heating of tritium in the DTE2 experiments reported in this paper is the lower tail temperature of ICRF-accelerated tritons as a consequence of different experimental conditions, i.e. higher plasma density and lower temperature and ICRF power. It resulted in improved bulk ion heating by ICRF heating and more peaked ICRF power deposition profiles.

A number of open questions remains after these DTE2 experiments that have been put forward to a possible future DTE3 campaign at JET. Prior to DTE2, a ^{3}He concentration in the range of ∼5% was considered necessary for ITER to achieve best ion heating conditions based on earlier experimental and modelling work, see e.g. [4–6]. The JET results presented in this paper together with earlier plasma confinement studies using ^{4}He [60] suggest, however, that lower levels of ^{3}He are better for overall plasma performance. Therefore, it would be necessary to further investigate the low ^{3}He regime with a ^{3}He concentration in the range of 0%–3% for ITER, to assess whether introducing ^{3}He is needed in ITER and, if it is, how much is sufficient. Furthermore, all DTE2 experiments were carried out with half of the NBI in tritium, which resulted in the absorption of approximately 10% ICRF power by tritium beam ions according to modelling (see section 4.6.1). Since there will be no tritium beams in ITER, doing experiments with D beams would provide a better match to ITER and allow the study of second harmonic T absorption as a function of plasma temperature in preparation of its use in ITER.

Acknowledgments

This work has been carried out within the framework of the EUROfusion Consortium, funded by the European Union via the Euratom Research and Training Programme (Grant Agreement No. 101052200-EUROfusion), the EPSRC (Grant No. EP/W006839/1), the Spanish National R&D Project PID2019-110854RB-I00/AEI/10.13039/501100011033, and Grant Nos. FIS2017-85252-R and PID2021-127727OB-I00 funded by MCIN/AEI/10.13039/501100011033 and ERDF 'A way of making Europe'. M.J.M. and D.G. from the Fusion Group at Barcelona Supercomputing Center are grateful for the support received from the Departament de Recerca i Universitats de la Generalitat de Catalunya with code 2021 SGR 00908. Views and opinions expressed are those of the author(s) only and do not necessarily reflect those of the European Union or the European Commission. Neither the European Union nor the European Commission can be held responsible for them.

ORCID iDs

M.J. Mantsinen https://orcid.org/0000-0001-9927-835X

D. Gallart https://orcid.org/0000-0003-1663-3550
P. Mantica https://orcid.org/0000-0001-5939-5244
D. Taylor https://orcid.org/0000-0002-0465-2466
D. Van Eester https://orcid.org/0000-0002-4284-3992
A. Dal Molin https://orcid.org/0000-0003-0471-1718
E. De La Luna https://orcid.org/0000-0002-5420-0126
R. Dumont https://orcid.org/0000-0002-1030-138X
J. Eriksson https://orcid.org/0000-0002-0892-3358
J. Garcia https://orcid.org/0000-0003-0900-5564
L. Garzotti https://orcid.org/0000-0002-3796-9814
J. Hobirk https://orcid.org/0000-0001-6605-0068
A. Kappatou https://orcid.org/0000-0003-3341-1909
V. Kiptily https://orcid.org/0000-0002-6191-7280
M. Lennholm https://orcid.org/0000-0002-3444-3999
C.F. Maggi https://orcid.org/0000-0001-7208-2613
M. Maslov https://orcid.org/0000-0001-8392-4644
R.B. Morales https://orcid.org/0000-0003-0667-3356
M. Nocente https://orcid.org/0000-0003-0170-5275
G. Pucella https://orcid.org/0000-0002-9923-2770
C. Reux https://orcid.org/0000-0002-5327-4326
D. Rigamonti https://orcid.org/0000-0003-0183-0965
S. Silburn https://orcid.org/0000-0002-3111-5113
E.R. Solano https://orcid.org/0000-0002-4815-3407
Z. Stancar https://orcid.org/0000-0002-9608-280X

References

[1] ITER Organization 2018 ITER Research Plan within the Staged Approach (Level III – Provisional Version) ITER Technical Report No. ITR-18-003 (available at: www.iter.org/doc/www/content/com/Lists/ITER%20Technical%20Reports/Attachments/9/ITER-Research-Plan_final_ITR_FINAL-Cover_High-Res.pdf)
[2] Phillips C.K. *et al* 1995 *Phys. Plasmas* **2** 2427
[3] McGuire K.M. *et al* 1995 *Phys. Plasmas* **2** 2176
[4] Start D.F.H. *et al* 1998 *Phys. Rev. Lett.* **80** 4681
[5] Start D.F.H. *et al* 1999 *Nucl. Fusion* **39** 321
[6] Eriksson L.-G. *et al* 1999 *Nucl. Fusion* **39** 337
[7] Rimini F.G. *et al* 1999 *Nucl. Fusion* **39** 1591
[8] Andrew P. *et al* 1999 *J. Nucl. Mater.* **266–269** 153
[9] Mailloux J. *et al* 2022 *Nucl. Fusion* **62** 042026
[10] Figueiredo J. *et al* 2016 *Rev. Sci. Instrum.* **87** 11D443
[11] Nocente M. *et al* 2022 *Rev. Sci. Instrum.* **93** 093520
[12] Vartanian S. *et al* 2021 *Fusion Eng. Design* **170** 112511
[13] Hobirk J. *et al* 2023 *Nucl. Fusion* **63** 112001
[14] Hobirk J. *et al* 2012 *Plasma Phys. Control. Fusion* **54** 095001
[15] Challis C.D. *et al* 2022 *48th EPS Conf. on Plasma Phys.* (*virtual, 27 June–1 July 2022*) *Europhysics Conference Abstracts Vol. 46A O1.101* (available at: http://ocs.ciemat.es/EPS2022PAP/pdf/O1.101.pdf)
[16] Maslov M. *et al* 2023 *Nucl. Fusion* **63** 112002
[17] Lerche E. *et al* 2023 Fundamental ICRF heating of Deuterium ions in JET-DTE2 *29th Fusion Energy Conf. (FEC2023)* (*London, UK, 16 – 21 October*)
[18] Kazakov Y. *et al* 2023 Plasma heating and fast-ion physics studies with three-ion ICRF scenarios in non-active and D-T plasmas on JET in support of ITER operations *29th IAEA Fusion Energy Conf. (FEC2023)* (*London, UK, 16 – 21 October 2023*)
[19] Garcia J. *et al* 2019 *Nucl. Fusion* **59** 086047
[20] Lerche E. *et al* 2020 *AIP Conf. Proc.* **2254** 030007
[21] Gallart D. *et al* 2020 *AIP Conf. Proc.* **2254** 060001
[22] Gallart D. *et al* 2018 *Nucl. Fusion* **58** 106037
[23] Kirov K.K. *et al* 2021 *Nucl. Fusion* **61** 046017
[24] Kirov K.K. *et al* 2019 *Nucl. Fusion* **59** 056005
[25] Mantsinen M.J. *et al* 2015 *42nd EPS Conf. on Plasma Physics* (*Lisbon, Portugal, 22–26 June 2015*) *Europhysics Conference Abstracts Vol. 39E P2.171* (available at: http://ocs.ciemat.es/EPS2015PAP/pdf/P2.171.pdf)
[26] Eriksson L.-G., Hellsten T. and Willén U. 1993 *Nucl. Fusion* **33** 1037
[27] Brambilla M. 1994 *Nucl. Fusion* **34** 1121
[28] Hawryluk R.J. 1980 An empirical approach to tokamak transport *Physics of Plasmas Close to Thermonuclear Conditions* vol 1, ed B. Coppi *et al* (CEC) pp 19–46
[29] Lamalle P.U. 1994 Nonlocal theoretical generalization and tridimensional numerical study of the coupling of an ICRH antenna to a tokamak plasma *PhD Thesis* LPP-ERM/KMS Report 101 Université de Mons
[30] Mantsinen M.J. *et al* 1999 *Plasma Phys. Control. Fusion* **41** 843
[31] Cottrell G.A. *et al* 1999 *Nucl. Fusion* **39** 389
[32] Stix T.H. 1975 *Nucl. Fusion* **15** 737
[33] Kazakov Y. *et al* 2017 *Nat. Phys.* **13** 973
[34] Garzotti L. *et al* 2023 Development of high current baseline scenario for high deuterium-tritium fusion performance at JET *Nucl. Fusion* submitted
[35] Sips A.C.C., Giruzzi G., Ide S., Kessel C., Luce T.C., Snipes J.A. and Stober J.K. 2015 *Phys. Plasmas* **22** 021804
[36] Polevoi A.R. *et al* 2015 *Nucl. Fusion* **55** 063019
[37] Graham M. *et al* 2012 *Plasma Phys. Control. Fusion* **54** 074011
[38] Monakhov I. *et al* 2013 *Nucl. Fusion* **53** 083013
[39] Durodié F. *et al* 2012 *Plasma Phys. Control. Fusion* **54** 074012
[40] Dumortier P. *et al* 2017 *Fusion Eng. Design* **123** 285
[41] Jacquet P. *et al* 2023 *AIP Conf. Proc.* **2984** 030003
[42] King D. *et al* 2023 *Nucl. Fusion* **63** 112005
[43] Frassinetti L., Beurskens M.N.A., Scannell R., Osborne T.H., Flanagan J., Kempenaars M., Maslov M., Pasqualotto R. and Walsh M. 2012 *Rev. Sci. Instrum.* **83** 13506
[44] Hawkes N.C., Delabie E., Menmuir S., Giroud C., Meigs A.G., Conway N.J., Biewer T.M. and Hillis D.L. 2012 *Rev. Sci. Instrum.* **89** 10D113
[45] Morales R.B. *et al* 2022 Improved accuracy and robustness of electron density profiles from JET's FMCW reflectometers *15th Int. Reflectometry Workshop for Fusion Plasma Diagnostics (IRW15)* (*ITER HQ, St Paul Lez Durance Cedex France, 7–10 June 2022*) (available at: www.aug.ipp.mpg.de/IRW/procpage.shtml)
[46] Lerche E. *et al* 2015 *J. Nucl. Mater.* **463** 634–9
[47] Sirén P., Beaumont P. and Weisen H. 2022 *J. Instrum.* **17** C08006
[48] Ericsson G., Ballabio L., Conroy S., Frenje J., Henriksson H., Hjalmarsson A., Källne J. and Tardocchi M. 2001 *Rev. Sci. Instrum.* **72** 759
[49] Andersson Sundén E. *et al* 2009 *Nucl. Instrum. Methods* A **610** 682
[50] Eriksson J., Conroy S., Andersson Sundén E. and Hellesen C. 2016 *Comput. Phys. Commun.* **199** 40
[51] Baeumel S. *et al* 2004 *Rev. Sci. Instrum.* **75** 3563
[52] Van Eester D. and Lerche E. 2011 *Plasma Phys. Control. Fusion* **53** 092001
[53] Kalupin D. *et al* 2013 *Nucl. Fusion* **53** 123007
[54] Strand P. *et al* 2018 *27th IAEA Fusion Energy Conf. (FEC 2018)* (*Gandhinagar, India, 22–27 October 2018*)

p TH/P6–14 (available at: https://nucleus.iaea.org/sites/fusionportal/Shared%20Documents/FEC%202018/fec2018-preprints/preprint0451.pdf)
[55] Challis C.D. *et al* 1989 *Nucl. Fusion* **29** 563
[56] Bilato R. *et al* 2014 *AIP Conf. Proc.* **1580** 291
[57] Bilato R. *et al* 2015 *AIP Conf. Proc.* **1689** 060001
[58] Budny R. *et al* 2012 *Nucl. Fusion* **52** 023023
[59] Dumont R. and Zarzoso D. 2013 *Nucl. Fusion* **53** 013002
[60] Kappatou A. *et al* 2017 *44th EPS Conf. on Plasma Physics* (*Belfast, Northern Ireland, UK*, *26–30 June 2017*) *Europhysics Conference Abstracts Vol. 41F O3.111* (available at: http://ocs.ciemat.es/EPS2017PAP/pdf/O3.111.pdf)